

Date of publication xxxx 00, 0000, date of current version xxxx 00, 0000.

Digital Object Identifier 10.1109/ACCESS.2017.Doi Number

# Reactive Power Control of PV Inverters in Active Distribution Grids with High PV Penetration

F. M. Aboshady<sup>1,2</sup> (Senior Member, IEEE), Ioana Pisica<sup>1</sup> (Senior Member, IEEE), Ahmed F. Zobaa<sup>1</sup> (Senior Member, IEEE), Gareth A. Taylor<sup>1</sup> (Senior Member, IEEE), Oguzhan Ceylan<sup>3</sup> (Member, IEEE) and Aydogan Ozdemir<sup>4</sup> (Senior Member, IEEE)

<sup>1</sup> Department of Electronic and Electrical Engineering, Brunel University, London United Kingdom (e-mail: Fathy.Aboshady@ieee.org, ioana.pisica@brunel.ac.uk, azobaa@ieee.org, gareth.taylor@brunel.ac.uk)

<sup>2</sup> Electrical Power and Machines Engineering Department, Tanta University, Tanta, Egypt (e-mail: Fathy.Aboshady@ieee.org)

<sup>3</sup> Department of Electrical and Electronics Engineering, Marmara University, Istanbul, Turkey (e-mail: oguzhan.ceylan@marmara.edu.tr)

<sup>4</sup> Department of Electrical Engineering, Istanbul Technical University, Turkey (e-mail: ozdemir@itu.edu.tr)

Corresponding author: Ioana Pisica (e-mail: ioana.pisica@brunel.ac.uk).

This work was supported by a Newton Fund Institutional Links grant, ID 623801791, under the Newton-Katip Çelebi Fund partnership. The grant is funded by the UK Department for Business, Energy and Industrial Strategy and TUBITAK grant ID 120N996 and delivered by the British Council.

**ABSTRACT** Photovoltaic (PV) systems can reduce greenhouse gas emissions while providing rapid reactive power support to the electric grid. At the distribution grid level, the PV inverters are controlled to reduce the system's active power loss and to address problems caused by the PV systems themselves. For example, the distribution grid may face overvoltages due to high PV generation during off-peak hours. In this paper, a reactive power control approach for PV inverters is proposed to control the injection/absorption of reactive power to reduce the active power loss of the system while solving the overvoltage problem. To achieve this, the proposed controller periodically dispatches the reactive power setpoints and applies a real-time volt/var algorithm. The proposed method uses probabilistic distributions to account for the uncertainties in PV generation and load demand. The controller is implemented at the lateral level which simplifies the required communication platform and reduces the computational cost. The real-time volt/var control coordinates the operation of the different inverters during overvoltage conditions so that the voltage rise is limited using as little reactive power as possible by the inverters. Accordingly, the active power loss due to reactive power flow in the system is reduced. Two distribution systems are simulated using Open Distribution System Simulator (OpenDSS) and used to evaluate the proposed controller and compare with two other methods. A daily time series simulation is performed to test different operating conditions. The simulation results show that the proposed controller is able to reduce the active power loss in general and solve the overvoltage problem with a lower reactive power requirement than the other volt/var methods.

**INDEX TERMS** Distribution network, photovoltaic, power loss minimization, smart inverters, volt/var control.

## I. INTRODUCTION

Renewable energy generation is increasing worldwide to reduce greenhouse gas emissions and their negative impact on the environment [1, 2]. For instance, the share of renewable energy in electricity generation was 42.8% in the United Kingdom in the fourth quarter of 2021 [3]. Photovoltaic (PV) systems, as a form of renewable energy source, have become widespread at the utility (solar farms) and end-use level (rooftops) [4]. PV systems are non-dispatchable sources where it is always desirable to extract the maximum active power/energy to increase the systems'

profitability[5]. Therefore, the continuous penetration of PV systems has brought challenges to system operation. For example, high PV generation in the distribution system during off-peak hours results in excess power flowing back to the main grid, exposing the distribution system to the risk of overvoltage [6]. Various control strategies have been developed using the smart PV inverters themselves to control the voltage. Research is also focused on using the reactive power capability of the PV inverters to improve the performance of the distribution grid through reducing the active power losses. The control methods reported in the

literature can be divided into local and communication-based methods, which are described with examples in the following subsections. It is worth noting that voltage regulation using conventional voltage regulators and capacitor banks is not considered in this study.

### A. LOCAL CONTROL

Local control methods use locally measured quantities such as the voltage and/or the generated power [7, 8] to limit the voltage rise. Several control methods were found in the literature, but the volt/var (reactive power control) and volt/watt (active power control) methods were most commonly used and described in the IEEE Std. 1547 [9]. Due to the high  $R/X$  ratio of the distribution system feeder, using the volt/watt control method for voltage regulation known as Active Power Curtailment (APC), would be more effective than using the volt/var control method [10, 11]. Despite its technical feasibility, it is not preferable from an economic point of view because the usable active energy is lost. Instead, APC has been used as a second solution when the reactive power control is not able to control the voltage alone, such as in the methods described in [10, 11] where a droop-based reactive power control was combined with APC.

In [12, 13], different local droop control methods were discussed and compared (e.g., voltage-dependent reactive power control method  $Q(V)$  and active power-dependent power factor control method  $\cos\phi(P)$ ). Then, a local droop control method combining  $Q(V)$  and  $\cos\phi(P)$  strategies was proposed to take advantage of the two methods. In [12], the characteristic of the standard  $\cos\phi(P)$  was adjusted according to the local voltage, resulting in  $\cos\phi(P,V)$ , while the reference reactive power of the inverter was generated as the weighted sum of the reactive power obtained from both  $Q(V)$  and  $\cos\phi(P)$  methods in [13]. Coordinated active power-dependent  $Q(P)$  and voltage-dependent  $Q(V)$  reactive power control methods were proposed in [14] and [15], respectively. In an attempt to not only overcome the overvoltage problem but also do so with a minimal active power loss due to reactive power flow, the authors coordinated the droop setting of the PV inverters along with the system. Voltage and power loss sensitivity matrices were constructed for the distribution network and used to coordinate the settings. In [15], the inverter setting parameters (threshold voltage, maximum reactive power, and the droop characteristic slope) were formulated in a multi-objective optimization problem and solved at an assumed critical point.

Local control methods avoid the use of communication networks and are therefore simple and inexpensive to implement. However, they do not consider the use of reactive power capability of PV inverters to reduce the grid losses and only consider voltage regulation. Despite efforts to locally coordinate the various inverters (e.g., [15]), the locally coordinated inverters may not provide the optimal solution under various conditions. In addition, different threshold parameters are required to implement these methods.

### B. COMMUNICATION-ASSISTED CONTROL

This type of control method employs the data collected from various locations via communication channels. Control can be centralized, while all data is sent to the central substation and processed. The voltage regulation elements are then given the control directives [16]. The advantage of centralized control approaches is that they provide a comprehensive overview of the distribution network. As a result, more effective/optimal control decisions can be made. A centralized control method applies optimization techniques to optimally allocate reactive power to the different inverters in the systems to overcome voltage violations and reduce active power loss of the system. For instance, in [17], the central controller coordinated the operation of conventional devices such as capacitor banks and voltage regulators with the smart inverters. The setting of the conventional devices was scheduled in an hourly timescale, while the setting of the inverters was done every 15 minutes.

Centralized control, on the other hand, requires a complex and costly communication infrastructure as well as knowledge of the system information, and involves a large amount of computation [18]. Moreover, these methods operate in a specific time window (dispatch interval) of a few minutes, during which the control decisions are assumed to be constant, which does not account for real-time system variations (e.g., changes in PV generation and its consequences during cloudy conditions) [19]. To address this shortcoming, the centralized control method was applied in [19] and coordinated with the local droop controllers, where the central controller solves an optimization problem to minimize system losses and dispatches the droop control settings to the local controllers. However, the central controller still requires an expensive communication network, and the computational cost is high [18].

In contrast to the use of a centralized controller with a complex communication network, a distributed control method for PV systems at the lateral level was proposed in [20]. The developed method relies on voltage and active power measurements along with the voltage sensitivity matrix to control the reactive power and use APC when needed to overcome the overvoltage problem. The need for power measurements increases the required communication bandwidth and cost. In [21], two communication-based modified droop control methods were proposed. The first method aims to equally share the reactive power and uses information about the reactive power of all inverters in the network to set the controller slope. In the second method, defined the droop slope was set by solving an optimization problem using the measured active power of all inverters to regulate the voltage and minimize the power loss. The second method showed better performance but was more expensive than the first method.

### C. CONTRIBUTION

In summary, the existing literature reveals a research gap in terms of local control methods not utilizing the reactive power capabilities of PV systems to minimize system losses. On the other hand, central control methods rely on complex and

costly communication systems, while also facing challenges due to the large size of the optimization problem, leading to increased computational requirements. Additionally, alternative distributed control methods have been reported, but they often necessitate multiple measurements, thereby raising implementation costs. In this paper, a new lateral-level reactive power control method for smart PV inverters is proposed. The proposed controller performs two main tasks:

1. Periodical dispatch of the inverter reactive power to minimize the active power losses along the lateral.
2. Real-time voltage control to overcome the overvoltage problem with minimum active power loss due to reactive power flow.

The proposed control method has the following characteristics:

1. Fast reactive power dispatch: it is applied at the lateral level; therefore, the problem size is smaller and simpler than the system level operation. In turn, the optimization problem can be solved faster which reduces the length of the dispatching interval (only 1-2 minutes).
2. Requires a simple communication system at the lateral level.
3. Scalability and flexibility: it can be replicated across many laterals to accommodate future system expansion. Unlike system level-operation, where the control method may need to be re-adjusted/reset to adapt to system configuration changes.
4. Setting-free: the proposed real-time volt/var controller does not require any predefined operating setting or characteristic, unlike the commonly used droop control methods.
5. Considers uncertainty and diversity of PV generation and load profiles along with the system. Often, a central controller assumes the same forecasted generation and/or demand for the entire system.

## II. PROPOSED CONTROLLER OVERVIEW

In this section, a general overview of the proposed controller is presented. The controller operates on the lateral level, as shown in Fig. 1, and performs two tasks that proceed with different time steps: a periodical dispatch of reactive power by solving an optimization problem and a real-time volt/var control, as shown in Fig. 2. At the beginning of each dispatch interval, the controller sets the reactive power of the different inverters along the lateral to minimize the active power losses. During the dispatch interval, the real-time volt/var controller monitors the lateral end-node voltage (or the voltage at the furthest downstream PV system) and adjusts the reactive power of the inverters, to overcome any voltage violation issues, if required. The communication requirements, as shown in Fig. 1, are limited to delivering the reactive power setpoints from the lateral controller to the inverters and monitoring the voltage at a point, where a simple low bandwidth communication link would suffice. The following two sections explain the two control objectives in detail.

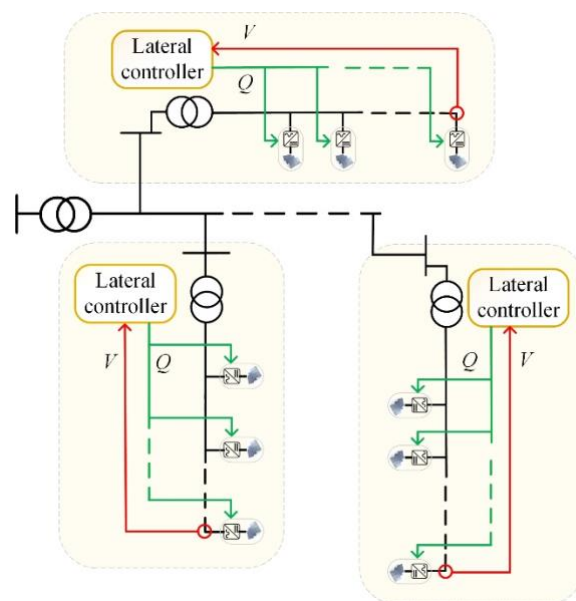


FIGURE 1. A distribution system with the proposed controller structure.

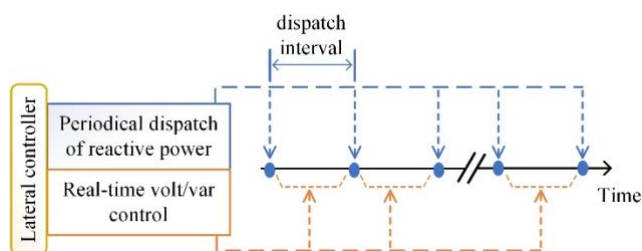


FIGURE 2. The timing diagram for the proposed controller.

## III. PERIODICAL DISPATCH OF REACTIVE POWER

The first task of the proposed controller is to periodically dispatch the reactive power of the PV systems to minimize the active power loss. In this regard periodical dispatch of reactive power is formulated as an optimal power flow where the objective function is the active power losses. The length of the dispatch time window (period) depends on the execution time of the optimal power flow problem, the prediction/forecasting time of the different variables (e.g., load and PV generation), and the communication time [19]. The system size and the corresponding number of nodes, lines, and PV systems (control variables) are major factors affecting the dispatch interval. For centralized control at the substation level, the dispatch interval varies from 15 to 60 minutes [19]. During this period, the system variables are assumed to be fixed. The proposed controller is applied at the lateral level, which has a limited size compared to the entire distribution network. Therefore, the dispatch interval can be much smaller (up to 1-2 minutes), as will be illustrated later. In the next subsections, the problem formulation, the uncertainty models, and the solution method are explained.

### A. PROBLEM FORMULATION

The optimization problem can be formulated as follows:

$$\min_{Q^{PV}} \sum_{ij} P_{ij}^{loss} \quad \forall ij \quad (1)$$

subject to:

$$\mathbf{I}_j = \sum_{k \in N} Y_{j,k} V_{k,t} \quad \forall j \quad (2)$$

$$P_j^{PV} - P_j^L = \text{Real}(V_j I_j^*) \quad \forall j \quad (3)$$

$$Q_j^{PV} - Q_j^L = \text{Imag}(V_j I_j^*) \quad \forall j \quad (4)$$

$$Q_i^{min} \leq Q_i^{PV} \leq Q_i^{max} \quad \forall i \quad (5)$$

$$V^{min} \leq V_j \leq V^{max} \quad \forall j \quad (6)$$

The objective function in (1) is to minimize the total active power loss along the lateral where  $P_{ij}^{loss}$  is the active power loss of the element connecting nodes  $i$  and  $j$ . The control variable is the reactive power of PV units,  $Q^{PV}$ . Regarding the power flow, the current injection  $\mathbf{I}_j$ , active and reactive power model for the PV ( $P_j^{PV}$ ,  $Q_j^{PV}$ ) and load ( $P_j^L$ ,  $Q_j^L$ ) at node  $j$  are represented by (2), (3), and (4), respectively, where  $Y$  is the system admittance matrix,  $V$  is the nodal voltage vector, and  $N$  is the number of nodes.

The upper and lower limits for the control variable  $Q^{PV}$  are given by (5). The PV inverter's reactive power capability is assumed to follow the minimum reactive power requirement as defined by the IEEE Std 1547-2018 [9], which is shown in Fig. 3, where  $Q^{max}$ , and  $Q^{min}$  are the limits for the reactive power injection and absorption respectively. The PV system is in an over-excited operating mode when it exhibits positive reactive power, while negative reactive power corresponds to an under-excited operation mode. The two points P1 and P2 in Fig. 3 correspond to the minimum active power generation under which there is no reactive power injection/absorption by the PV system, and the minimum active power generation that allows injecting/absorbing the maximum reactive power, respectively. The standard values for P1 and P2, as a percentage of the PV rated power ( $P^{rate}$ ), are 5% and 20%, respectively [9]. The upper and lower limits are defined in (7) as a function of the PV system active power, where  $S^{rate}$  is the inverter rated apparent power and the + refers to  $Q^{max}$  while the - refers to  $Q^{min}$ . When the active power is greater than 5% and less than 20% (*Otherwise* case in (7)), the relationship between the reactive power and the active power is a straight line with a slope of  $(0.44 S^{rate} \div 0.2 = 2.2 S^{rate})$  as depicted in (7). As it can be noticed, the inverter rated power is larger than the PV rated power to allow injecting/absorbing reactive power even when the PV is generating its maximum power [9].

$$Q_i^{max,min} = \begin{cases} 0 & P_i^{PV} < 0.05 P_i^{rate} \\ \pm 0.44 S_i^{rate} & P_i^{PV} \geq 0.2 P_i^{rate} \\ \pm 2.2 S_i^{rate} \cdot P_i^{PV} & \text{Otherwise} \end{cases} \quad \forall i \quad (7)$$

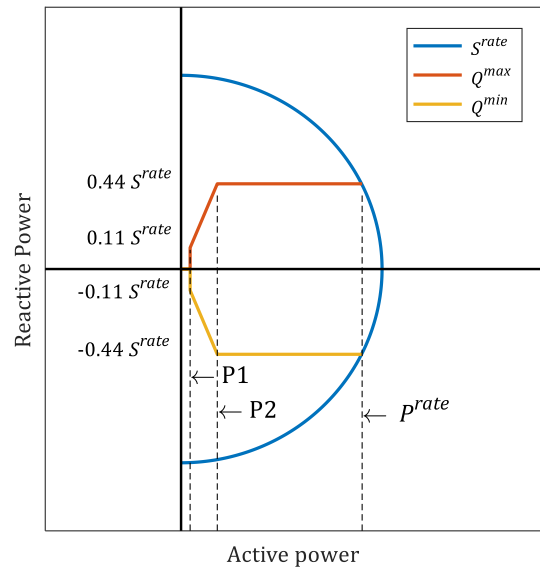


FIGURE 3. The reactive power capability of the PV inverters [9].

The nodal voltage is a dependent variable with its limits set by (6). The voltage limits depend on the system voltage level and the employed standard [22]. The inequality constraint in (6) is maintained by adding it to the objective function in (1) as a quadratic penalty term [23]. Therefore, the objective function in (1) is modified to (8), where  $\lambda$  is the penalty factor. The power loss and the nodal voltage in (8) are represented as per-unit (pu) quantities.

$$\min_{Q^{PV}} \left[ \sum_{ij} P_{ij}^{loss} + \sum_j \lambda (V_j - V^{limit})^2 \right] \quad (8)$$

where

$$V^{limit} = \begin{cases} V^{min} & V_j < V^{min} \\ V^{max} & V_j > V^{max} \\ V_j & \text{Otherwise} \end{cases} \quad (9)$$

## B. UNCERTAINTY IN PV GENERATION AND LOAD

To solve the previously formulated optimal power flow problem, PV generation and the load demand are needed. One possible option used in the literature is using forecasted values [24]. However, even with forecasted values, uncertainties associated with the irradiance and load demand must be considered [25]. For this purpose, probabilistic modeling of these parameters was used. The irradiance and the load demand are often represented by Beta and Gaussian probability distributions, respectively [19, 25-29]. In

addition, in [28, 29] the irradiance measurements were used directly to construct the uncertainty model instead of relying on the forecast model which requires a large database of historical data [26] to construct and other data, such as last week's estimates, to run. After constructing the uncertainty models for different variables, the problem can be solved using different approaches, such as Monte Carlo simulation and scenario-based analysis, which are accurate but computationally intensive [19, 25]. Another way to solve the problem is to divide the distribution grid into several stages/regions and estimate a weighted average value for these stages/regions according to their probability [27-29]. This approach involves a low computational effort than the previous solution.

The literature provided the forecasting and uncertainty models for the central substation, assuming the same irradiance and load values as for the entire system. The length of the dispatch interval (often 15 to 60 minutes [19]) is influenced by the prediction time [19]. It is clear that a fixed irradiance level and the same load patterns for the distribution grid along the dispatch interval do not reflect the actual operating conditions.

The proposed controller operates at the lateral level, which covers a small region when compared to the entire distribution system. Therefore, the approximation of assuming the same forecasted value along the lateral would be more realistic than along the entire distribution system. Regarding the irradiance level, we assumed the availability of an irradiance meter (similar to [28, 29]) at the lateral level to provide a few measurements to the controller, which are then used to model the stochastic nature of the solar irradiance as will be illustrated. Since, the proposed controller is applied at the lateral level, it has access to the lateral measurements of the main transformer. Therefore, using the actual measurements of transformer power ( $P^{XFMR}$ ) and irradiance (the corresponding PV generation  $P^{PV}$ ), a plausible estimate for the aggregate load power ( $P^L$ ) can be made if the lateral power loss ( $P^{loss}$ ) in (10) is ignored. An average load demand for various loads along the lateral is then estimated. This estimate does not match actual load demand, but is a simpler alternative to using a load forecasting model, which also cannot estimate the actual load demand. The estimated load points are then used to create the Gaussian distribution to account for the uncertainty in the load demand. The irradiance ( $G$ ) and active power generation, ignoring the temperature effect, are related by (11), where  $G_{std}$  is the irradiance under the standard conditions (1000 W/m<sup>2</sup>), and  $R_c$  is a specific irradiance point (150 W/m<sup>2</sup>) [30, 31].

$$\sum P^L = P^{XFMR} + \sum P^{PV} - \sum P^{loss} \quad (10)$$

$$P^{PV}(G) = \begin{cases} p^{rate} \cdot \frac{G^2}{G_{std} \cdot R_c} & 0 < G < R_c \\ p^{rate} \cdot \frac{G}{G_{std}} & G \geq R_c \end{cases} \quad (11)$$

In such a case, the whole process of estimating PV generation and load demand depends mainly on the frequency of irradiance measurements, which allows a significant reduction of the dispatch interval. The dispatch interval can be as low as 1-2 minutes, which is an advantage for the proposed controller. The measurements during a given time interval and the corresponding uncertainty models are used to estimate the variable values for the next time interval. It is worth mentioning that the estimated irradiance and corresponding PV generation are used to adjust the upper and lower limits for reactive power according to (7).

#### 1) PV GENERATION UNCERTAINTY MODEL

The Beta distribution function is used to characterize the uncertainty in the solar irradiance (12) [26, 27].

$$f_b(G) = \frac{\Gamma(\alpha + \beta)}{\Gamma(\alpha) \cdot \Gamma(\beta)} \cdot G^{(\alpha-1)} \cdot (1 - G)^{(\beta-1)} \quad (12)$$

where

- $f_b(G)$  Beta probability density function;
- $G$  irradiance in kW/m<sup>2</sup> ( $0 \leq G \leq 1$ );
- $\alpha, \beta$  Beta distribution shape parameters ( $\alpha, \beta \geq 0$ );
- $\Gamma$  Gamma function.

The shape parameters ( $\alpha, \beta$ ) are calculated from the irradiance data for every time interval using the mean ( $\mu$ ) and the standard deviation ( $\sigma$ ) values of the irradiance during that interval as follows.

$$\beta = (1 - \mu) \cdot \left( \frac{\mu \cdot (1 + \mu)}{\sigma^2} - 1 \right) \quad (13)$$

$$\alpha = \frac{\mu \cdot \beta}{1 - \mu} \quad (14)$$

The generated irradiance distribution is divided into  $M$  region segments (between the minimum and maximum irradiance values), as shown in Fig. 4. The irradiance for each region is calculated as the average of the region boundaries ( $G_1, G_2, \dots, G_M$ ). The probability of each region ( $\rho_1, \rho_2, \dots, \rho_M$ ) is calculated (area under the curve), either by integrating  $f_b(G)$  over the region boundaries or approximately using the trapezoidal rule. Then, the effective irradiance ( $G^{eff}$ ) is calculated as a weighted sum for different regions, using the probability of the region as a weighting factor (15). Finally, the corresponding PV

generation for different PVs along the lateral is estimated by (11).

$$G^{eff} = \sum_{m=1}^M G_m \cdot \rho_m \quad (15)$$

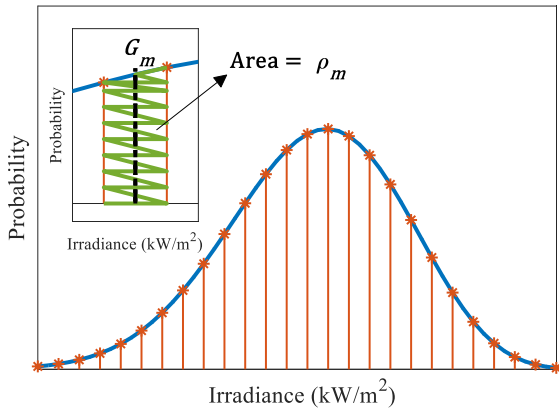


FIGURE 4. Probability distribution of the solar irradiance.

## 2) LOAD UNCERTAINTY MODEL

As explained earlier, the PV generation estimated with (11) at different measured irradiance values can be used together with the transformer lateral active power measurement to obtain the load's active power values with using (10), ignoring the losses. These load values are used to construct the Gaussian distribution  $f_n(d)$  which characterizes the load uncertainty (16), where  $\mu$  and  $\sigma$  are the mean and standard deviation of the load values of the current time interval, and ( $d$ ) refers to the load demand. Then, the effective load demand is estimated similarly to the effective irradiance mentioned above. It is assumed that the reactive power follows the same distribution as of the active power, which is a practical assumption used in the literature [19].

$$f_n(d) = \frac{1}{\sigma\sqrt{2\pi}} \cdot \exp\left[-\frac{(d - \mu)^2}{2\sigma^2}\right] \quad (16)$$

## C. SOLUTION METHOD

Two tools/methods are required to solve the problem: a load flow method and an optimization method. For the purpose of this paper neither the load flow method nor the optimization method to be used will be compared or selected. Different load flow methods can be used for distribution systems [32, 33]. Moreover, the optimization problem can be solved using different approaches, e.g., nature-inspired algorithms such as the Genetic Algorithm and Particle Swarm Optimization [34]. The field of optimization is subject to continuous development. New improved methods have been developed by combining two original methods [28].

This paper uses the Open Distribution System Simulator (OpenDSS) [35] to model the distribution network under study and solves the load flow problem at different candidate

solutions. Briefly, the OpenDSS is based on the construction of the system admittance matrix that relates the node voltages and currents. Starting from an initial guess of the node voltages, the problem is then solved iteratively until it converges. It is suitable for both balanced and unbalanced distribution systems.

The Pattern Search optimization method [36, 37] is adopted in this paper as it requires fewer function evaluations compared to the evolutionary methods. It should be noted that other methods can also be used and compared. The Pattern Search method can be seen from Fig. 5 in which the algorithm creates a pattern/grid of trial points around the base point (the best solution so far). Initially, the current point is the base point, and the method solves the problem at the trial points. At each iteration, the pattern either moves its base point to a new point (a point with a better objective function value) or shrinks in size if no better solution is found. This process continues until reaching the stop criteria. More details on the theory and implementation of the method can be found in [36, 37]. MATLAB is used to model the proposed controller and has been interfaced with the OpenDSS.

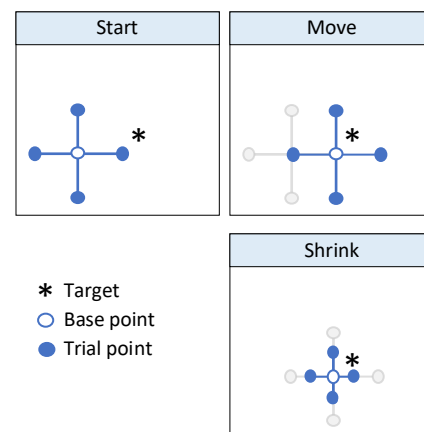


FIGURE 5. Illustration of Pattern Search showing pattern movement and shrinking.

## IV. REAL-TIME VOLT/VAR CONTROL

While the optimal dispatch of reactive power takes place at regular intervals, the controller also monitors the voltage in real-time and coordinates the operation of various PV inverters to avoid any voltage violations. The distribution system suffers from an overvoltage problem especially when PV generation is high during off-peak hours [13, 20]. The surplus PV generation causes in a reverse power flow in the system, which in turn pushes the voltage to rise at nodes further away from the substation. The solution to the overvoltage problem is the focus of this part of the paper.

The overvoltage problem is solved by utilizing the reactive power capability of the smart PV inverters along the lateral. Since this is a real-time application, it would not be advisable to rely on solving the optimal power flow because solving the optimization problem requires time. Therefore, in this section a different approach is proposed to solve the

overvoltage problem. The previous section has shown that PV inverters are set to certain reactive power values during the dispatch interval to minimize the power loss. If an overvoltage problem occurs during this interval, the real-time volt/var control algorithm responds to bring the voltage back to the accepted limits. The proposed controller aims to do this while minimizing the loss incurred. This task can be accomplished by disturbing as small a number of inverters as possible from their previously dispatched reactive power.

The proposed approach is to change the reactive power of one inverter at a time, then another inverter if necessary. The nodal voltage variation due to reactive power variation (injection/absorption) increases while moving downstream from the main substation [13, 38]. Therefore, the proposed controller alters the reactive power setpoint for the inverter located furthest downstream along the lateral first. With a reverse power flow, the voltage at the most downstream PV system connection point has the highest level along the lateral [15]. The proposed controller monitors the voltage of that connection point. Once the monitored voltage exceeds the permitted upper voltage limit, determined by the system voltage level and the corresponding standard [22], the controller modifies the reactive power setpoint for the inverter. In the presence of an overvoltage, the inverter reduces its injected reactive power (if it was previously over-excited) or even starts absorbing reactive power (operates in an under-excited mode). As explained earlier, the overvoltage problem occurs when PV generation is high. For this reason, and based on the characteristics in Fig. 3, the limit for the reactive power of each inverter is  $-0.44$  pu. The controller modifies the inverter's reactive power setpoint until the voltage returns to the accepted limit or the inverter reaches its reactive power limit. If the inverter absorbs its maximum reactive power, but the voltage still exceeds the limit, the controller starts to modify the reactive power setpoint for another inverter. This procedure is repeated until the problem is solved. The real-time volt/var control operates based on a straightforward concept that monitors the voltage and adjusts the inverter's reactive power setpoint accordingly. This simplistic volt/var control approach facilitates the adherence of the proposed controller to real-time operations.

The implementation procedure of the proposed controller with both operating stages (periodic dispatch of reactive power and real-time volt/var control) is depicted in Fig. 6. The change in reactive power ( $\Delta Q$ ) can be a fixed value (e.g., 0.05 pu), or it can be quantitatively tied to the current-voltage deviation from the voltage limit, with the larger the deviation, the higher the  $\Delta Q$ . A fixed-step of 0.05 pu was used in this study.

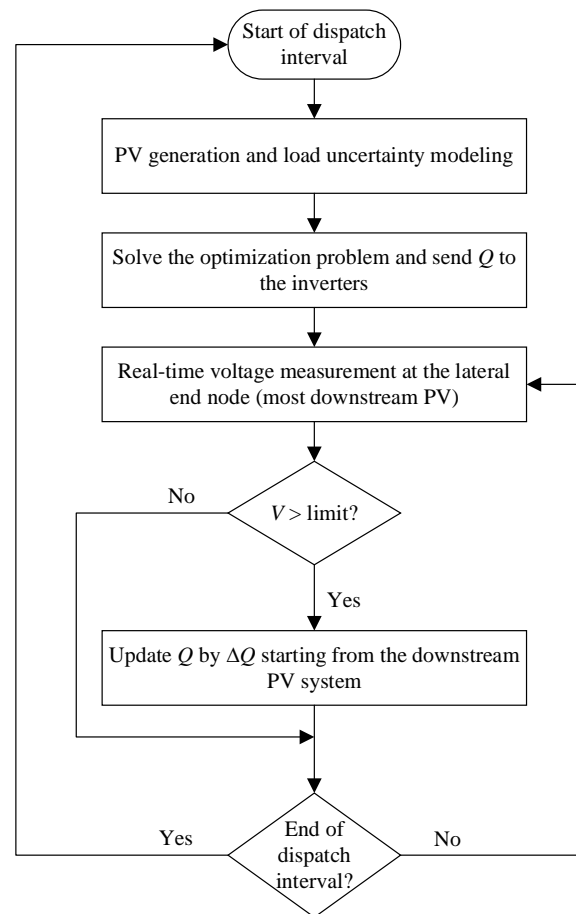


FIGURE 6. Implementation procedure of the proposed controller.

## V. SIMULATION STUDY

The performance of the proposed controller is evaluated in this section. The proposed volt/var controller is compared with the state of art volt/var control method of the IEEE Std 1547 [9] and with the optimally designed volt/var controllers in [15].

### A. TEST SYSTEMS

Two test systems have been used for the simulation studies: a simple, balanced system comprising a single low voltage lateral which was previously used in [15], and a modified version of the IEEE 13-bus medium voltage feeder [39, 40].

#### 1) SIMPLE TEST SYSTEM

The first test system is shown in Fig. 7, which consists of 5 buses connected to the medium voltage (MV) grid through a distribution transformer. The system data is given in Table I [15]. This system is used as an illustrative example to compare the proposed volt/var control method and the other methods.

#### 2) MODIFIED IEEE 13-BUS TEST SYSTEM

A modified IEEE 13-bus feeder is used for the extensive evaluation of the proposed controller. The single-line diagram of the modified system is shown in Fig. 8. The original IEEE 13-bus feeder is a medium voltage system (4.16 kV). It has been modified to include low voltage

laterals connected to the medium voltage feeder through distribution transformers. In order to evaluate only the performance of the smart PV inverters other voltage control elements were removed or kept at fixed settings. Therefore, the voltage regulator present in the original system at the main substation was left at a fixed tap setting. The capacitor banks were also removed.

The modified system has five three-phase laterals. Two of these have with balanced loads and are connected to buses 671 and 680 in Fig. 8. The other three laterals have unbalanced loads and are connected to buses 634 and 675 (2 laterals). Six single-phase laterals were added on different phases along the system and connected to buses 692, 652, 611, 645, and 646 (2 laterals). Data for the medium voltage IEEE 13-bus feeder can be found in [39]. The general construction of all low voltage laterals follows the system in Fig. 7. The lateral data is given in Table II, with all the three-phase laterals having the same transformer and cable data and similarly to the single-phase laterals.

TABLE I  
PARAMETERS OF THE TEST SYSTEM 1

Element	Parameters
Medium voltage grid	20 kV, 100 MVA, $X/R=1$
Distribution transformer	20/0.4 kV, 250 kVA, $Z=4\%$
Cable section	150 m, $Z=0.346+j0.0754 \Omega/\text{km}$

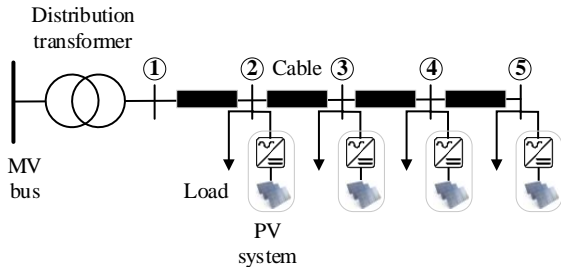


FIGURE 7. A simple low voltage test system.

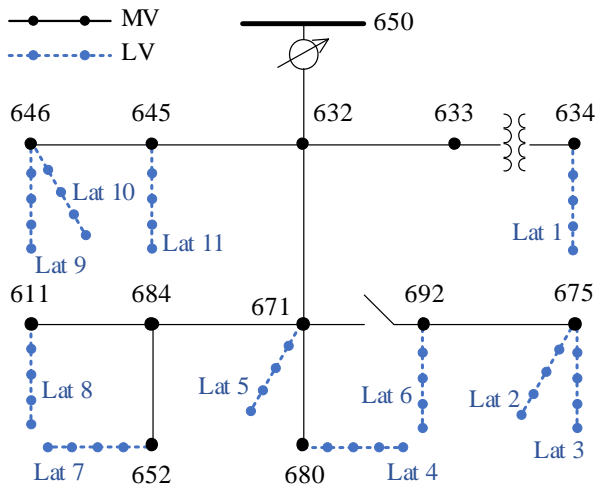


FIGURE 8. A modified version of the IEEE 13-bus feeder.

TABLE II  
PARAMETERS OF THE LATERALS IN TEST SYSTEM 2

Element	Parameters
Three-phase transformer	4.16/0.48 kV, Y/Y, 500 kVA, $X=2\%$ , $R=1.1\%$
Single-phase transformer	2.4/0.277 kV, 150 kVA, $X=2\%$ , $R=1.1\%$
Three-phase cable section	50 m, $Z_s=0.114+j0.0359 \Omega/\text{km}$ , $Z_m=0.0228+j0.0072 \Omega/\text{km}$
Single-phase cable section	50 m, $Z=0.14+j0.0357 \Omega/\text{km}$

### B. EVALUATION ON THE SIMPLE SYSTEM

Firstly, the proposed controller is evaluated in different operating scenarios. Then, the proposed volt/var controller is compared to the IEEE Std 1547 volt/var control method [9] and the method developed in [15] that optimally coordinates the setting of different PV inverters.

#### 1) EVALUATION

Testing scenarios can be hypothetically defined or derived from real operation data. Here we have derived them from a one-year recorded data in the U.K. [41]. The original data, involving 17520 demand-generation scenarios, have been clustered and aggregated into 26 representative scenarios [41]. Six of these scenarios correspond to variation of the load demand during periods of no PV generation (e.g., nighttime) and accordingly, were not included in the study. The other 20 scenarios are presented in Table III. Each entry in Table III represents the period for which the corresponding scenario extends during the year as a percentage of the annual number of hours (8760). For instance, the entry for the first scenario is 0.04, which means this scenario occurs for  $0.04/100 \times 8760 = 3.5$  h during the year. It can be noticed that the 20 scenarios represent 44.42% of the year while the omitted six scenarios cover the rest of the year, as previously mentioned.

TABLE III  
DEMAND-GENERATION SCENARIOS

% of PV generation	20	30	50	70	90	100
10	①0.04	②3.35	③12.32	④7.41	⑤2.64	⑥0.08
30	⑦0.01	⑧0.64	⑨10.89	⑩1.31	⑪0.07	
50		⑫0.09	⑬4.00	⑭0.18		
70		⑮0.05	⑯1.20	⑰0.01		
90			⑱0.11	⑲0.01		
100			⑳0.01			

① refers to the scenario number from 1 to 20.

The load at different buses was assumed to be 30 kW with 0.9 lagging power factor. To easily sense the values, the PVs had the same rated power as the loads. The grid voltage was set to 1.02 pu. The system was tested under these 20 scenarios. For each scenario, the PV inverters operated at a unity power factor of one and operated at the dispatched reactive power following the proposed controller commands on another occasion. The accepted voltage upper and lower

limits depend on the voltage level and the operating standard. For the comparison later in this section, the accepted voltage margin for this system is assumed to be  $\pm 10\%$  [15, 42].

The voltage magnitudes of the buses (the main grid is bus 0) for different scenarios are shown in Fig. 9 when the PV inverters were running at the unity power factor. Since all the voltage magnitudes are within the specified limits, the real-time volt/var controller has not been activated for any scenario. Hypothetical test conditions will be used in the comparison subsection later to evaluate the performance of the proposed real-time volt/var controller. When employing the reactive power dispatch controller, the corresponding voltage profiles are shown in Fig. 10. Both figures clearly show that the voltage increases when moving away from the main grid (bus 0) for a few scenarios. This emphasizes the reverse power flow from the PVs to the main grid when the PV generation exceeds the loading level. For that reason, the distribution grid suffers from overvoltage at far nodes when the PV generation is high during off-peak loading periods.

To show the benefit of the reactive power dispatch, the total system active power loss (objective function) is compared with and without reactive power control. The percentage decrease in active power loss due to reactive power control is calculated by (17) and is depicted in Fig. 11 for different scenarios. The following observations can be derived from Fig. 11.

- Reactive power dispatch decreases the active power loss in all scenarios because it reduces the need to transfer the reactive power from the main grid to the loads.
- In three scenarios where the PV generation was equal to the load demand, all the load power was locally generated, leading to almost zero active power loss or a 100% decrease in loss.
- The percentage decreases in losses are relatively small for the first six scenarios. The reason for that is the increase in demand (accordingly, reactive power requirement) while the PV generation is 10%, and accordingly, the inverter reactive power is limited to 50% of its reactive power limit following the characteristics in Fig. 3.

The reactive power of the PV inverters for different scenarios is shown in Fig. 12.

$$\%Decrease = \frac{Original - Control}{Original} \times 100 \quad (17)$$

Table IV The active power loss in various scenarios, both with and without reactive power control, is presented in second and third columns in Table IV. As expected, the power loss escalates with higher load levels. An example of this can be observed when transitioning from scenario 1 to 6, where the load percentage increased from 20% to 100% of the peak demand, leading to increased losses. However, in all cases, the implementation of reactive power control effectively reduces the active power loss. Notably, in scenarios such as 13 and 17, where the load power was

entirely supplied by the PV systems, the feeder experienced zero loss.

Table IV is multiplied by the corresponding value in Table III. This allows for different weighting the scenarios. Then, the average kW loss during the PV generation period of the year (sum/44.42) without and with reactive power control is calculated as 2.483 kW and 1.747 kW, respectively. The average active power loss for this system has decreased by 29.64% over the entire PV generation period (44.42% of the year) when the proposed reactive power control is used.

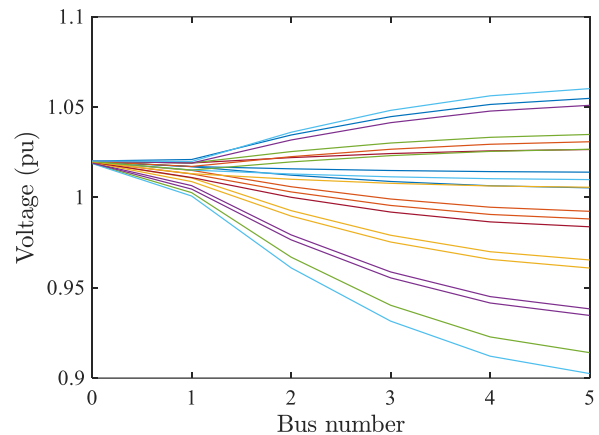


**FIGURE 9.** Voltage profiles when the PV inverters operate at unity power factor.

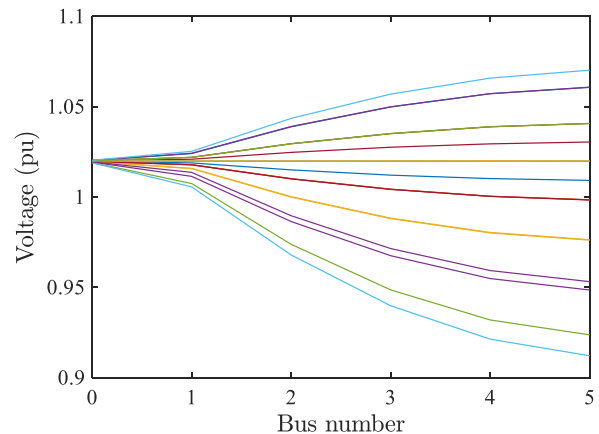


**FIGURE 10.** Voltage profiles when the PV inverters operate at the dispatched reactive power levels.

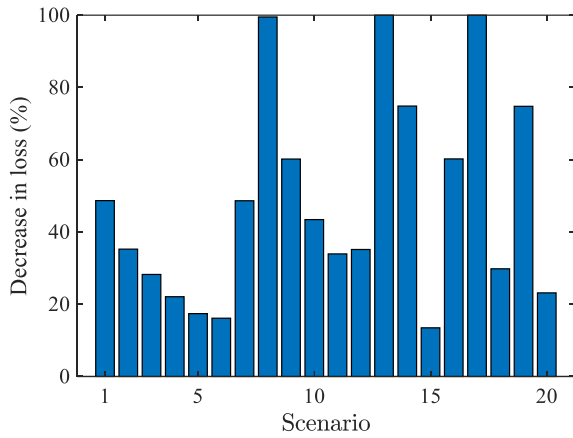


FIGURE 11. Percentage decrease in active power loss in different scenarios.

TABLE IV  
ACTIVE POWER LOSS FOR DIFFERENT SCENARIOS

Scenario	kW loss		Scaled kW loss	
	w/o Q	with Q	w/o Q	with Q
1	0.189	0.097	0.008	0.004

2	0.610	0.395	2.044	1.323
3	2.284	1.639	28.139	20.192
4	5.069	3.950	37.561	29.270
5	8.524	7.041	22.503	18.588
6	10.49	8.798	0.839	0.704
7	0.183	0.094	0.002	0.001
8	0.203	0.001	0.130	0.001
9	0.992	0.395	10.803	4.302
10	2.897	1.639	3.795	2.147
11	5.807	3.837	0.406	0.269
12	0.569	0.369	0.051	0.033
13	0.569	0	2.276	0
14	1.570	0.395	0.283	0.071
15	1.626	1.407	0.081	0.070
16	0.925	0.368	1.110	0.442
17	1.123	0	0.011	0
18	1.983	1.392	0.218	0.153
19	1.463	0.369	0.015	0.004
20	2.727	2.096	0.027	0.021

Final average		2.483	1.747
---------------	--	-------	-------

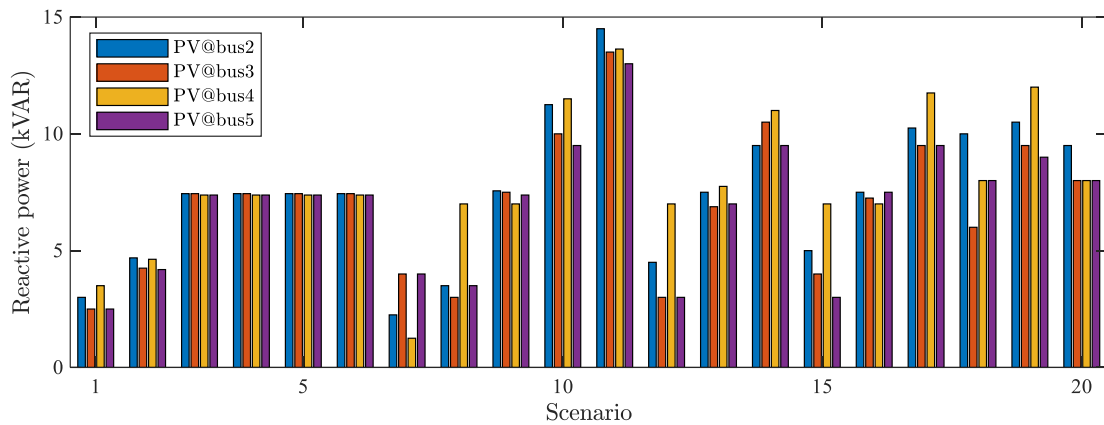


FIGURE 12. Dispatched reactive power for different PV inverters in different scenarios.

## 2) COMPARISON

The proposed real-time volt/var controller is compared to the state of art volt/var control method reported in the IEEE Std 1547-2018 [9] and the optimally coordinated volt/var control method in [15]. The volt/var characteristic used in [9, 15] to overcome the overvoltage problem in the distribution system through absorption of reactive power (under-excited mode) is shown in Fig. 13. Briefly, the inverter absorbs a certain amount of reactive power according to the characteristic in Fig. 13 if the voltage exceeds  $V_3$ . The maximum reactive power is absorbed if the voltage reaches/exceeds  $V_4$ .

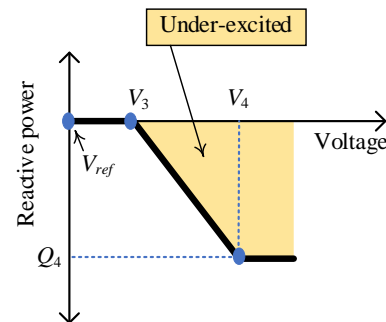


FIGURE 13. Voltage-reactive power characteristic in under-excited mode [9].

In [9], a default setting and the acceptable range for the voltage breaking points are defined. No specific rules were mentioned to select the setting for different inverters in the system. On the other hand, the settings for different

inverters were optimally coordinated in [15]. Two methods were developed in [15]: assuming equal reactive power share between the inverters and unequal share based on a multi-objective optimization problem. As the latter provided better performance, it has been used in the comparison.

To comply with the work presented in [15] and to test under the same conditions, the low voltage system in Fig. 7 has been modified as follows:

1. A PV system was added at bus 1;
2. All the loads were removed.

In an unloaded system, the generated PV power flows directly into the main grid. Therefore, the voltage level in the system increases. The default setting is used for all inverters when applying the IEEE 1547 method ( $V_3=1.02$  pu and  $V_4=1.08$  pu) because it has shown a good performance under different operating conditions [8, 9]. The inverter setting as derived in [15] is shown in Table V. This setting is the outcome of solving a multi-objective optimization problem [15]. Note that the per-unit reactive power limit is referred to the PV-rated power, not the inverter-rated apparent power. As is clear, the PV system connected at bus 1 is not sharing in the reactive power control. The voltage upper limit used in [15], which is 1.1 pu according to the EN 50160 [42], has been used in this comparison.

TABLE V  
PV INVERTER SETTING FOR THE METHOD IN [15]

PV Bus	1	2	3	4	5
$V_3$ (pu)	1.023	1.054	1.073	1.087	1.094
$V_4$ (pu)	1.026	1.056	1.078	1.093	1.1
$ Q_d $ (pu)	0	0.207	0.484	0.484	0.484

The total PV generation has been increased from 50 kW to 150kW. The generated power flowed to the main grid leading to voltage rise along the lateral as shown in Fig. 14. The voltage at bus 4 and bus 5 exceeded the upper limit (1.1pu) above a certain generation level when the PV inverters were operating at a unity power factor. Three control methods were applied to solve the problem, namely, the proposed method (Proposed), the method in [15] (Samadi), and the IEEE Std 1547 method (IEEE 1547). The voltage at the final bus (bus-5) is depicted in Fig. 15 for the three control methods. All the methods successfully solved the overvoltage problem that existed for the original unity power factor case. The IEEE 1547 method reduced the voltage level even for the low PV penetration levels where there was no voltage violation problem. This will be reflected in the utilized amount of reactive power during the control operation. The total reactive power absorbed by all the PV systems is shown in Fig. 16, where the negative sign refers to reactive power absorption. The proposed method shows the lowest reactive power utilization to overcome the overvoltage problem, followed by the optimized method by Samadi *et*

*al* [15]. Note that reactive power flow to bring the voltage down to the limit increases the active power loss. The increase in the active power loss due to reactive power as a percentage of the no reactive power flow cases is estimated and presented in Fig. 17. Because the proposed method requires the lowest reactive power, it results in the lowest increase in the active power loss compared to the other methods. The IEEE 1547 shows the highest power loss as it starts reactive power injection even for the no voltage violation conditions. The increase in loss for the IEEE 1547 method decreases at the high PV generation because the absolute increase in power loss is almost fixed, and when referred to the power loss at unity power factor, which is increasing, it shows a decreasing percentage. It is worth noting that as the active power generation increases to 150kW, it becomes necessary for different PV systems to absorb reactive power close to their limits. For that reason, the proposed method and the method proposed by Samadi come closer at higher PV generation levels. Nevertheless, the proposed method is still providing the lowest reactive power requirement. For the aim of illustrating the activation of the PV inverter's control one by one when using the proposed method, Fig. 18 shows the reactive power for two PV systems. It is clear that the PV inverter at bus 4 is activated only when the downstream inverter reaches its reactive power limit (14.5 kVAR in this study).

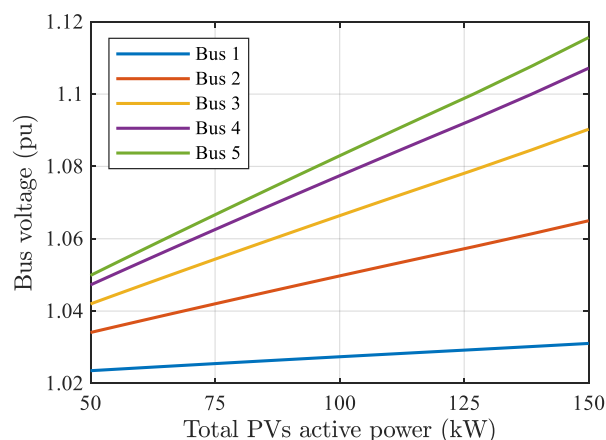


FIGURE 14. Voltage profile at unity power factor for different PV generation.

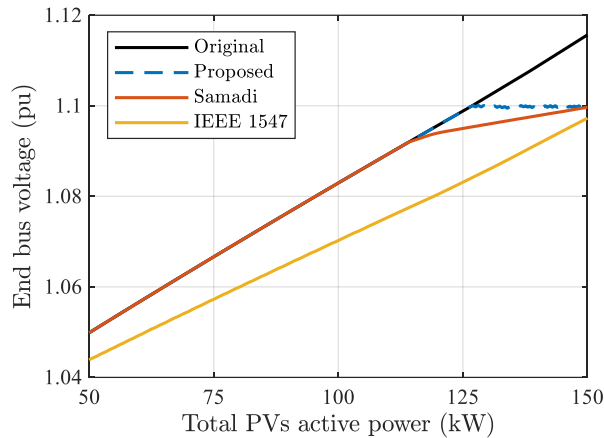


FIGURE 15. Voltage at the end bus when applying different control methods.

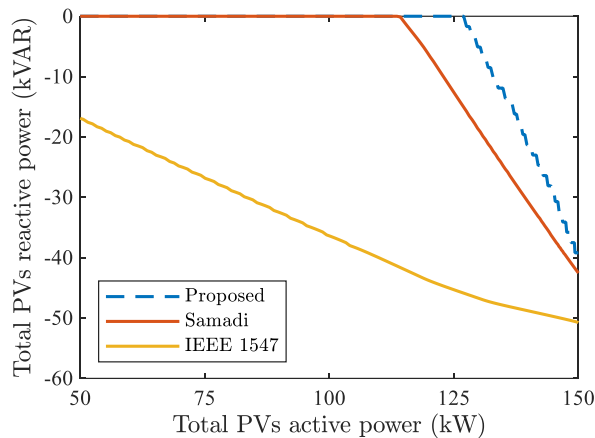


FIGURE 16. Reactive power utilization when applying different control methods.

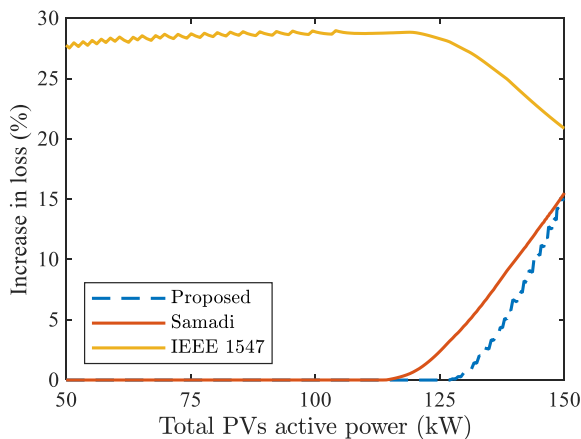


FIGURE 17. Increase in active power loss when applying different control methods.

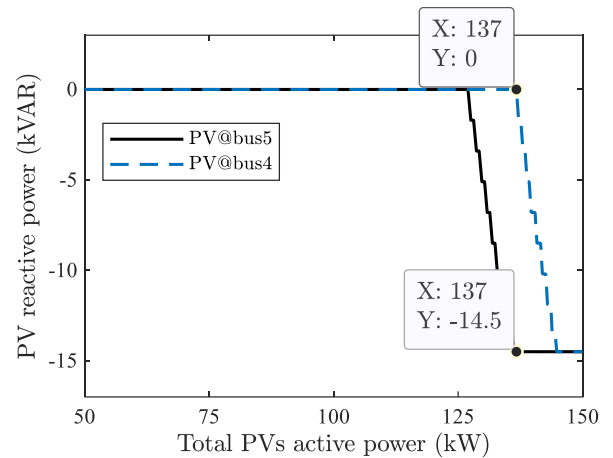
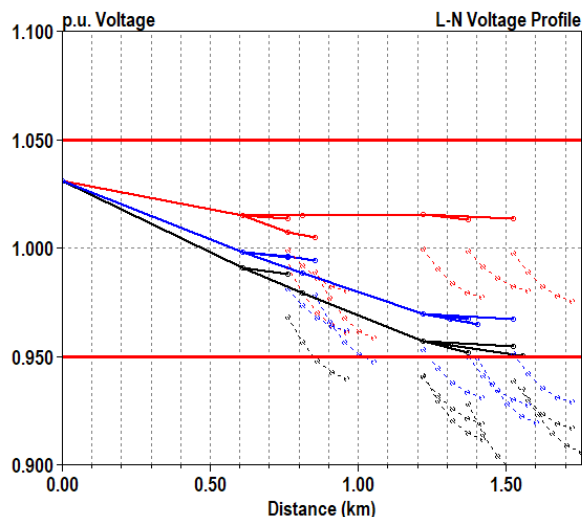


FIGURE 18. Reactive power for two PV systems when applying the proposed control method.

### C. EVALUATION ON THE MODIFIED IEEE SYSTEM

The modified IEEE 13-bus feeder shown in Fig. 8 was used as an unbalanced system. A high PV penetration level of 96% of the total load capacity was used by installing PVs at different nodes along the low voltage laterals. This level of PV penetration remains within the limits of both the feeder capacity and the substation transformer capacity. The voltage profiles for the system without PV generation, i.e., the loads fed from the main substation, are shown in Fig. 19. The distance is measured from the main substation at bus 650. The medium voltage (MV) feeder sections and the low voltage (LV) laterals are represented by continuous and dashed lines, respectively. The voltage profile reflects the unbalanced nature of the system. As previously mentioned, the substation regulator is maintained at a fixed tap position (that provides 1.03 pu in this study), and the capacitor banks are removed to check the influence of the smart PV inverters on the system performance. In this part of the simulation study, the voltage upper and lower limits for the LV laterals are 1.05 pu and 0.95 pu, respectively, in accordance with the ANSI C84.1 specifications [22]. Many low voltage nodes fall below the lower voltage limit—particularly for phase A (black) and phase C (blue). The incorporation of PV systems enhanced the voltage profile, as shown in Fig. 20. The choice of voltage level at the substation should be noted as arbitrary, but a value of 1.03 pu was selected due to its ability to maintain voltage within acceptable limits at all nodes when considering PV active power generation.



**FIGURE 19.** Voltage profile for the modified IEEE 13-bus feeder without PV generation (black=phase A, red=phase B, blue=phase C, continuous =MV, and dashed=LV).

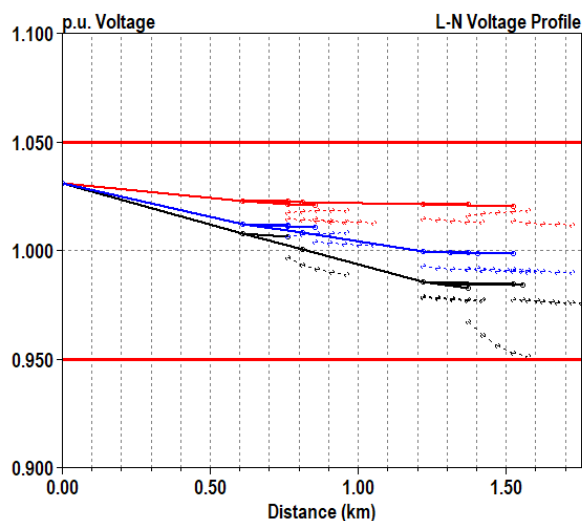


**FIGURE 20.** Voltage profile for the modified IEEE 13-bus feeder with PV generation (black=phase A, red=phase B, blue=phase C, continuous=MV, and dashed=LV).

Daily time series simulation was performed. Previous studies often assumed the same irradiance level and/or load profiles for the whole system [20]. In this study, three different irradiance profiles, which are shown in Fig. 21, were generated by the tool developed in [43]. Therefore, different PV systems were subjected to different irradiance levels. Also, different load profiles reported for the European low voltage test feeder in [39] were used. A sample of the load profiles is shown in Fig. 21. In this study, the dispatch interval used is 2min. The operation of the real-time volt/var control is then illustrated by an example.

Firstly, simulation results while the PV inverters were operating at unity power factor are presented, then when employing the proposed reactive power controller. The total daily active power loss (1440 minutes) along all the

laterals and the individual daily energy loss for different laterals are shown in Fig. 22 at the unity power factor. The first five laterals show higher energy loss because they are three-phase laterals (higher loading). The voltage profiles across the laterals are shown in Fig. 23 to Fig. 29. The voltages at the start and end buses of each lateral are presented. For three-phase laterals, the voltage of different phases is shown. It can be noticed from the profiles that:

- There are some periods of overvoltages along all the laterals due to high PV generation and reverse power flow. This is clear as the voltage at the end bus exceeds the upper voltage limit (1.05 pu).
- There are some periods of undervoltage along a few laterals—particularly phase A and/or phase C (e.g., laterals 2 and 3) due to high loading conditions while there is limited/no PV generation. Noting that the inverters are not sharing any reactive power yet.

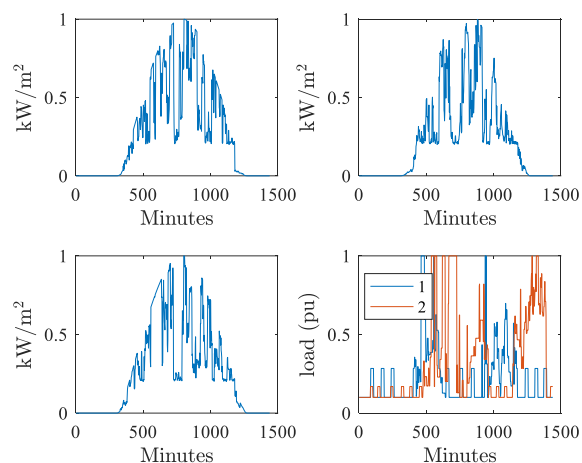


**FIGURE 21.** Three irradiance profiles and two load profiles.

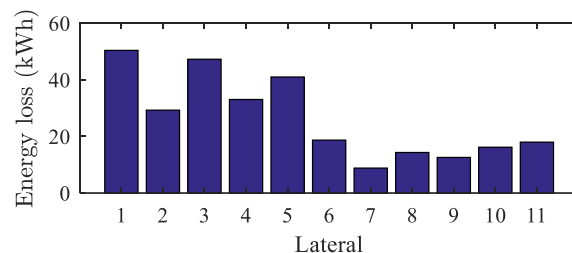
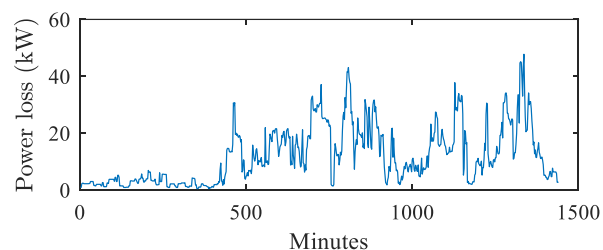


**FIGURE 22.** Power and energy loss when the PV inverters operate at unity power factor.

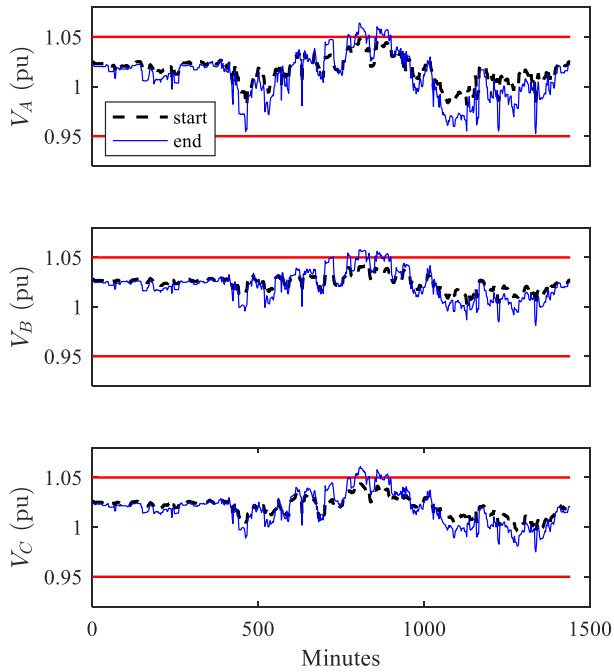


FIGURE 23. Voltage profile along lateral 1 when the PV inverters operate at unity power factor.

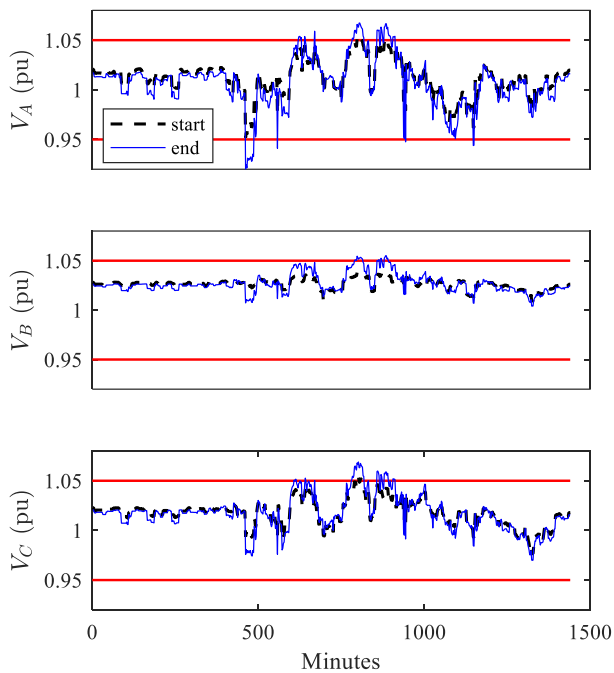


FIGURE 24. Voltage profile along lateral 2 when the PV inverters operate at unity power factor.

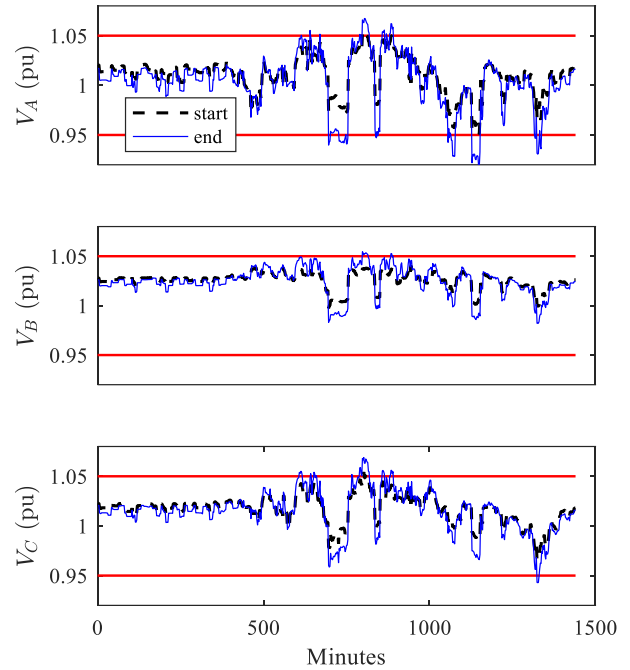


FIGURE 25. Voltage profile along lateral 3 when the PV inverters operate at unity power factor.

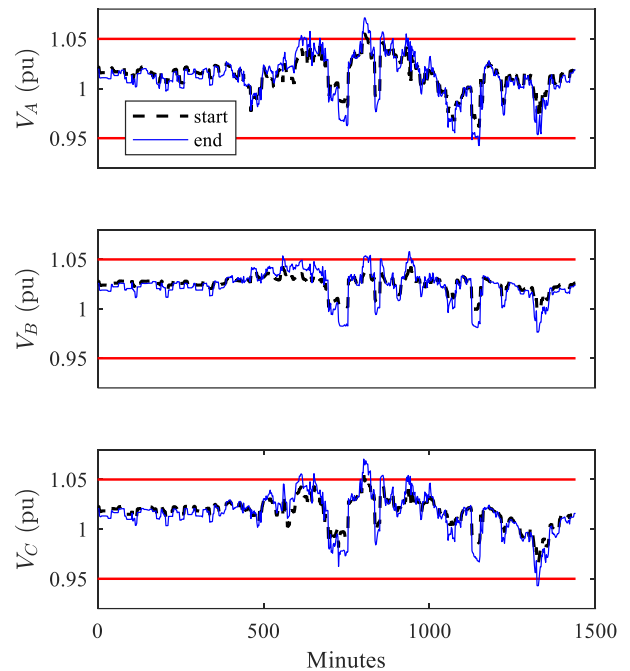


FIGURE 26. Voltage profile along lateral 4 when the PV inverters operate at unity power factor.

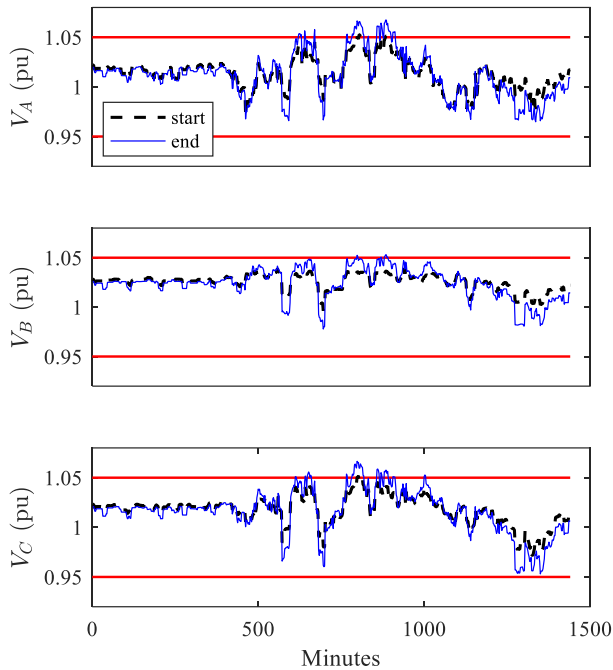


FIGURE 27. Voltage profile along lateral 5 when the PV inverters operate at unity power factor.

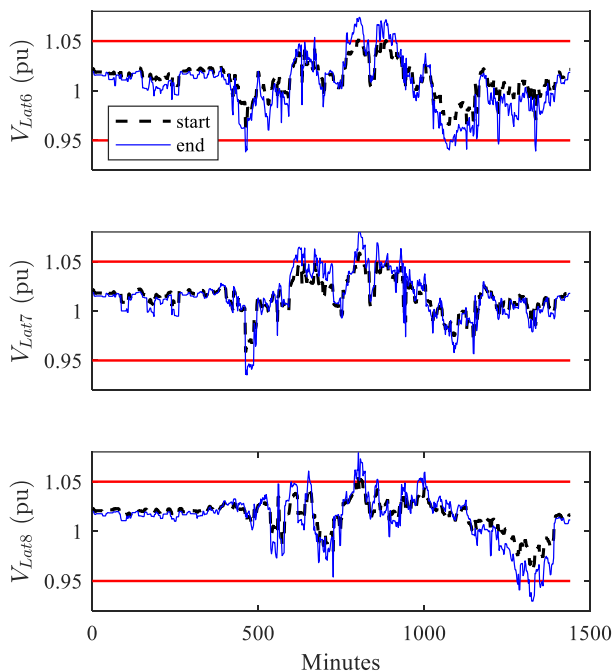


FIGURE 28. Voltage profile along laterals 6, 7, and 8 when the PV inverters operate at unity power factor.

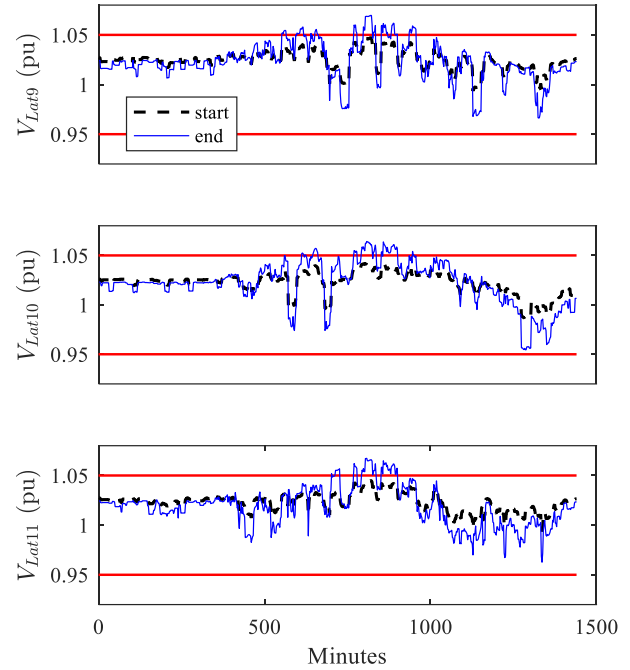


FIGURE 29. Voltage profile along laterals 9, 10, and 11 when the PV inverters operate at unity power factor.

When the proposed reactive power controller was employed, the inverters injected/absorbed reactive power following the controller commands. The active power and the energy losses are compared to the unity power factor cases as depicted in Fig. 30 and Fig. 31, respectively. The percentage decrease in a loss estimated by (17) and shown in Fig. 30 shows three trends:

- 1- Zero values (no decrease in losses) following the characteristic in Fig. 3, during the periods when the PV generation was below 5% of the rated power. During these periods, there was no reactive power-sharing by the PV inverters.
- 2- Positive values (decrease in losses) where the PV inverters were injecting reactive power into the system leading to a reduction in the imported reactive power from the main grid to feed the loads.
- 3- Negative values (increase in losses) where the PV inverters were under-excited and absorbing reactive power from the system when the system voltage was violating the upper voltage limit (overvoltage conditions). The additional reactive power flow increased the active power loss.

Nevertheless, there was net energy saving over the entire simulation period, as illustrated in Fig. 31. Comparing the total energy loss (kWh) in both cases, applying the proposed controller resulted in a daily reduction in energy loss by 13.7% under the used test conditions.

The voltage at the end bus of each lateral, which suffers from overvoltage or undervoltage at unity power factor as presented in Fig. 23 to Fig. 29, has been recorded and displayed in Fig. 32 to Fig. 38 when applying the proposed

control method. From the voltage profiles, it can be derived that:

- 1- The reactive power controller overcame all the overvoltage problems along the laterals.
- 2- The controller also solved the undervoltage problem for different situations.
- 3- There are still periods of undervoltage where the PV systems were not generating any reactive power (e.g., lateral 3). For such times of the day, operation of other voltage regulation devices such as transformer online tap changer would be needed.

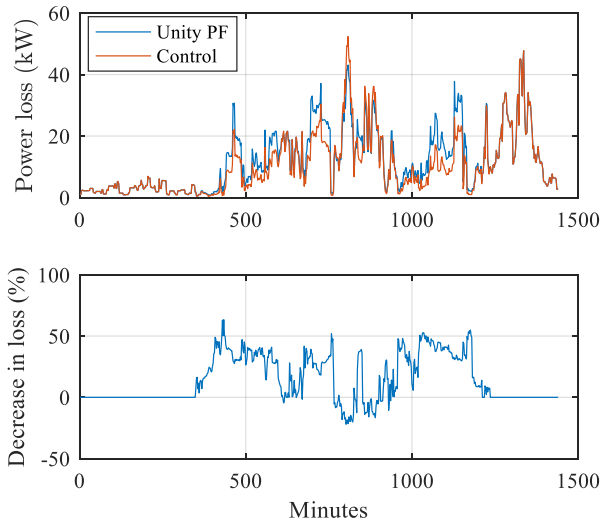


FIGURE 30. Active power loss with and without control.

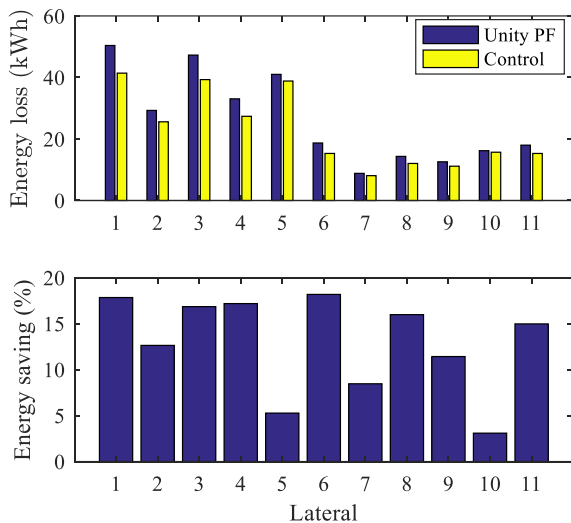


FIGURE 31. Energy loss with and without control.

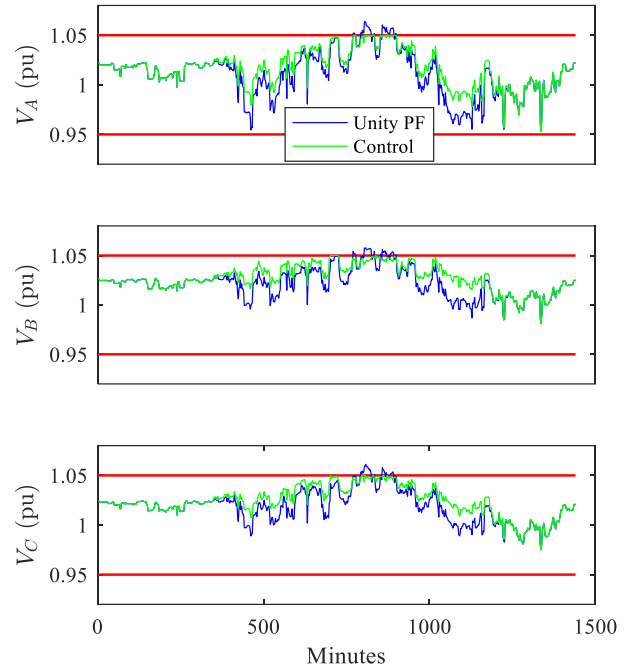


FIGURE 32. Voltage profile at end bus of lateral 1 with and without control.

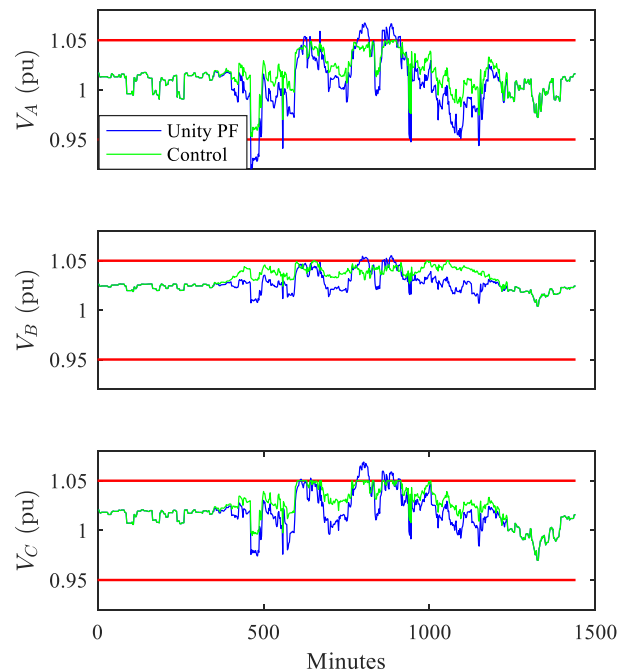
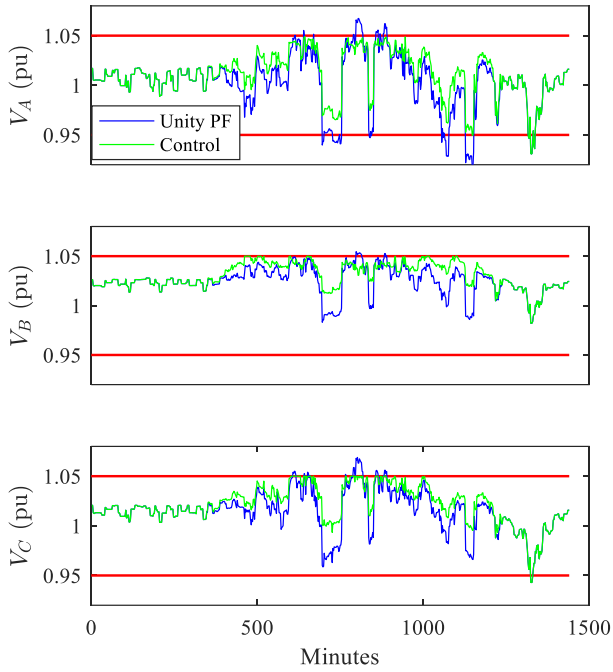
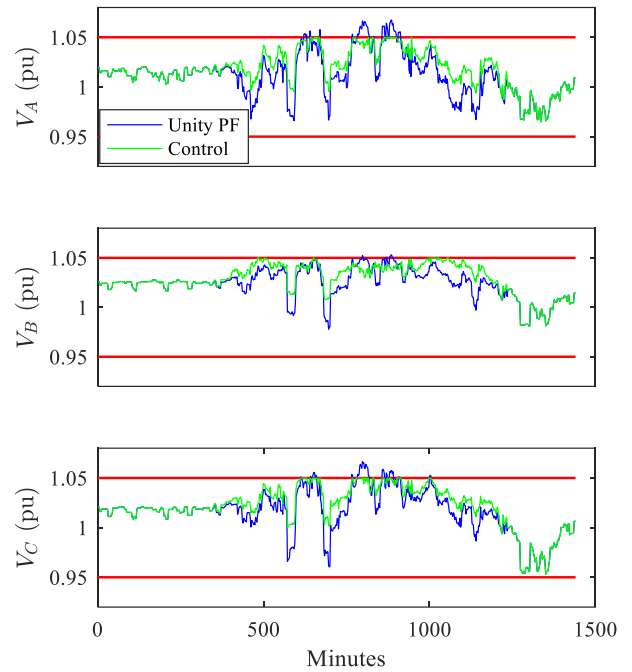


FIGURE 33. Voltage profile at end bus of lateral 2 with and without control.



**FIGURE 34.** Voltage profile at end bus of lateral 3 with and without control.



**FIGURE 36.** Voltage profile at end bus of lateral 5 with and without control.

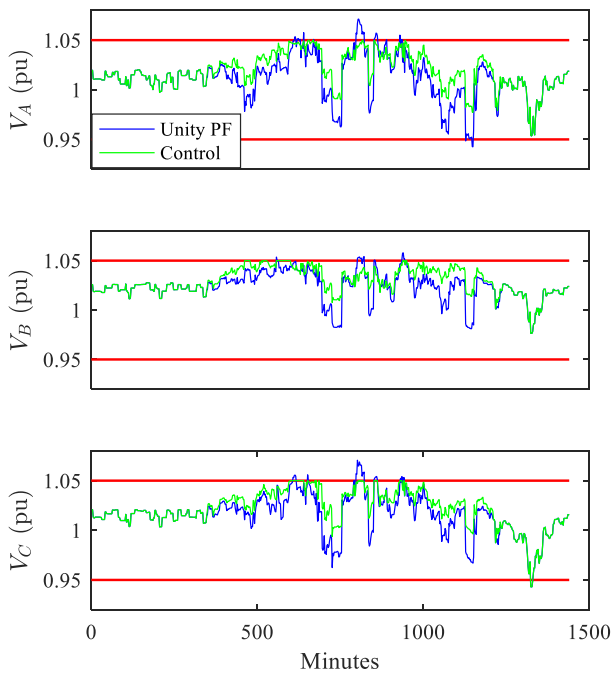


**FIGURE 35.** Voltage profile at end bus of lateral 4 with and without control.

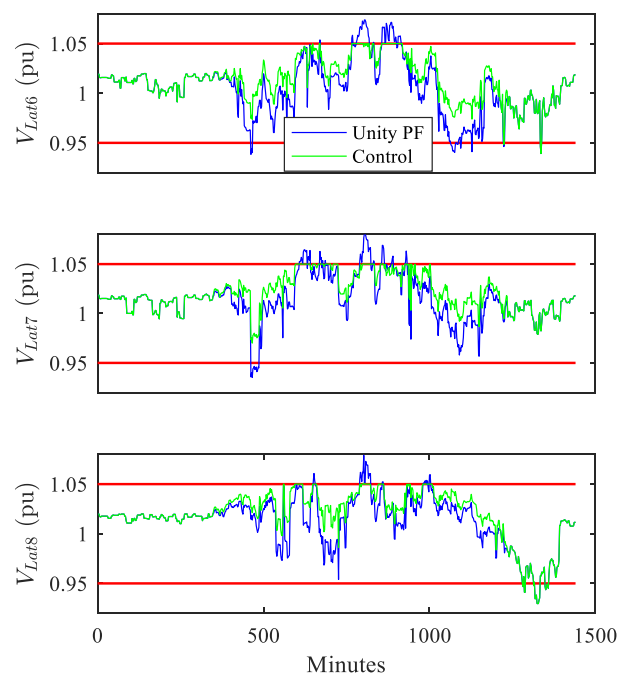


**FIGURE 37.** Voltage profile at end bus of laterals 6, 7, and 8 with and without control.

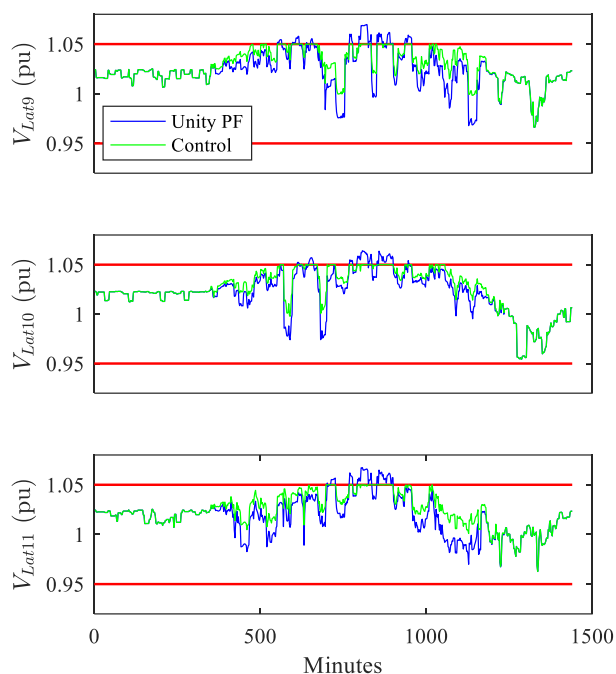


**FIGURE 38.** Voltage profile at end bus of laterals 9, 10, and 11 with and without control.

As explained earlier, the proposed real-time volt/var control operates within the dispatch interval to solve any voltage violation issue that may arise. Otherwise, the inverters would continue with the same dispatched reactive power until the next dispatch interval starts. To illustrate this process, one dispatch interval (2 minutes) has been expanded in 5 second increments. The resolution can be less than 5s, but this is for illustrative purposes only. Accordingly, the dispatch interval has been divided into 24 sub-intervals in which the real-time volt/var control operates. A dispatch interval during the midday was used (around 12 pm). The irradiance values at the beginning of the dispatch interval (first sub-interval) follow the values used for the optimal dispatch process. Then, hypothetical values were used for the other sub-intervals, as shown in Fig. 39. For simplicity, the load was assumed to be constant during the whole 2-minute period.

Higher irradiance at the same loading level results in voltage rise in the system if not considered. The voltage along a few laterals increased, exceeding the upper voltage limit (1.05pu) when exposed to the irradiance profiles in Fig. 39. Employing the proposed real-time volt/var control can handle this problem. For instance, the voltage at the end bus of lateral 7 and lateral 8 with and without real-time volt/var control are shown in Fig. 40. The volt/var controller modified the reactive power commands to the PV systems starting from the initial values dispatched by the optimal reactive power dispatch problem. Examples of the modification of the reactive power for two PV systems on each lateral are shown in Fig. 41 and Fig. 42. The real-time volt/var controller changed the reactive power for only one PV unit on lateral 7 to solve the overvoltage

problem. On the other hand, it required the participation of two PV systems on lateral 8. It is clear that the PV system changed the mode of operation from over-excited (injection) to under-excited (absorption). This result emphasizes the role of the proposed real-time volt/var controller in conjunction with the periodical dispatch of reactive power.

The simulation study presented in the previous two subsections proves the validity of the proposed concept and shows its technical advantages. To illustrate the advantage of the proposed controller in reducing the computational burden, an example is presented using the modified IEEE 13-bus system shown in Fig. 8. The computational demands, including CPU load and memory requirements, directly depend on the size of the optimization problem. The problem size is determined by the number of control variables involved. In the system, there are a total of 11 laterals, and each lateral is simulated to consist of 4 PV systems, which translates to 4 control variables. Consequently, a central controller would need to solve an optimization problem involving 44 control variables. In contrast, the proposed controllers at the lateral level only deal with 4 control variables each. This substantial difference in the size of the optimization problem results in a significant reduction in computational load.

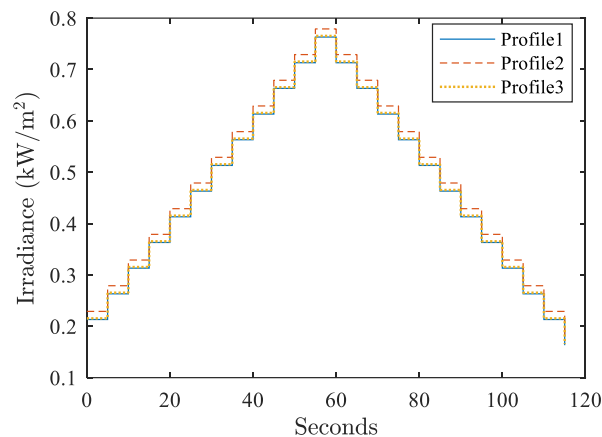


**FIGURE 39.** Irradiance variation during one dispatch interval at midday.

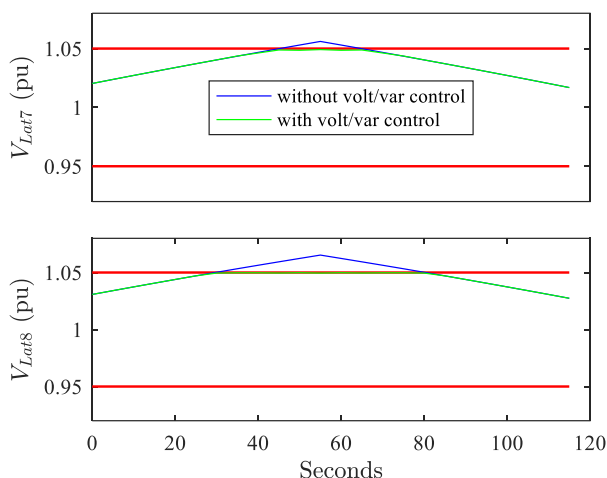


FIGURE 40. Voltage profile with and without real-time volt/var control.

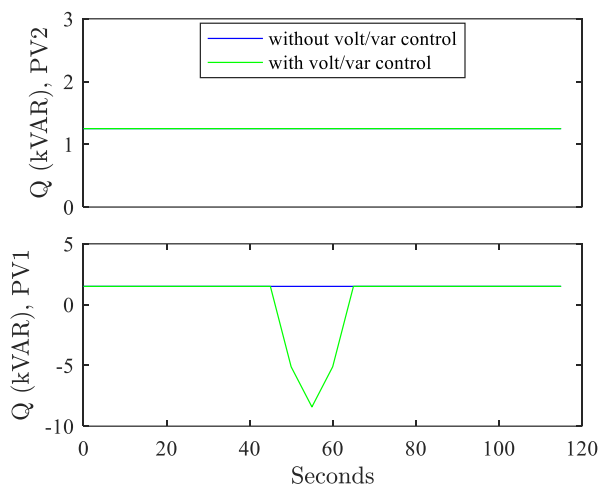


FIGURE 41. Variation in reactive power for two PV systems on lateral 7.

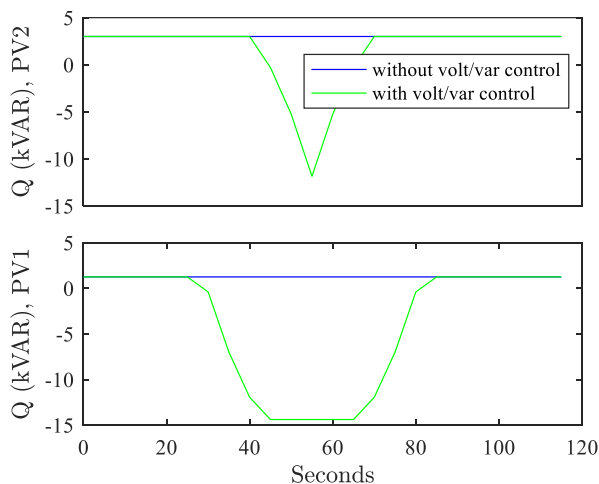


FIGURE 42. Variation in reactive power for two PV systems on lateral 8.

## VI. CONCLUSION

Current standards for distributed energy resources interconnecting consider their participation in voltage regulation. This paper has proposed a reactive power

controller that uses the capabilities of the spreading PV inverters to improve the performance of the distribution network. The controller was responsible for two tasks: periodic dispatch of reactive power to reduce active power loss in the system and real-time volt/var control to overcome overvoltage circumstances. The proposed controller operates at the lateral level, which reduces the computing load, dispatch interval, and communication requirements. The real-time volt/var control recursively and progressively updates the reactive setpoint of the PV inverters to solve the overvoltage problem while keeping the incurred associated power loss as low as possible. Unlike the droop control methods, the proposed controller does not require predefined setting parameters or operating characteristics. Also, it can be replicated across many laterals to accommodate future system expansion.

A simulation study was conducted on two tests systems. A simple balanced test system was used to prove the concept and compare its performance with of the other methods. The proposed volt/var controller outperformed the IEEE Std 1547 volt/var control method and an optimally designed volt/var control method in terms of reactive power need and active power loss associated with handling the overvoltage problem. A modified version of the unbalanced IEEE 13-bus feeder was employed for extended testing. Daily simulation has been performed. The results demonstrated the efficiency of the proposed controller in reducing the system loss and overcoming the voltage violations (both undervoltage and overvoltage). The controller cannot solve the undervoltage during periods of no/limited PV generation (e.g., at night), because there is no reactive power source. During these times, other voltage control devices, such as an online tap changer, can be utilized to regulate the voltage.

## REFERENCES

- [1] A. Qazi *et al.*, "Towards sustainable energy: A systematic review of renewable energy sources, technologies, and public opinions," *IEEE Access*, vol. 7, pp. 63837-63851, 2019.
- [2] R. M. Elavarasan *et al.*, "A comprehensive review on renewable energy development, challenges, and policies of leading Indian states with an international perspective," *IEEE Access*, vol. 8, pp. 74432-74457, 2020.
- [3] Department for Business, Energy and Industrial Strategy, (24/5/2022). *Energy Trends: UK renewables* [Online]. Available: <https://www.gov.uk/government/statistics/energy-trends-section-6-renewables>.
- [4] R. A. Shayani and M. A. G. de Oliveira, "Photovoltaic generation penetration limits in radial distribution systems," *IEEE Transactions on Power Systems*, vol. 26, no. 3, pp. 1625-1631, 2011.
- [5] X. Li, Q. Wang, H. Wen, and W. Xiao, "Comprehensive studies on operational principles for maximum power point tracking in photovoltaic systems," *IEEE Access*, vol. 7, pp. 121407-121420, 2019.
- [6] H. Sun *et al.*, "Review of challenges and research opportunities for voltage control in smart grids," *IEEE Transactions on Power Systems*, vol. 34, no. 4, pp. 2790-2801, 2019.
- [7] J. W. Smith, W. Sunderman, R. Dugan, and B. Seal, "Smart inverter volt/var control functions for high penetration of PV on distribution systems," in *2011 IEEE/PES Power Systems Conference and Exposition*, 2011, pp. 1-6.

- [8] M. Rylander, H. Li, J. Smith, and W. Sunderman, "Default volt-var inverter settings to improve distribution system performance," presented at the 2016 IEEE Power and Energy Society General Meeting (PESGM), Boston, MA, 17-21 July, 2016.
- [9] "IEEE Standard for Interconnection and Interoperability of Distributed Energy Resources with Associated Electric Power Systems Interfaces," *IEEE Std 1547-2018 (Revision of IEEE Std 1547-2003)*, pp. 1-138, 2018.
- [10] S. Ghosh, S. Rahman, and M. Pipattanasomporn, "Distribution voltage regulation through active power curtailment with PV inverters and solar generation forecasts," *IEEE Transactions on Sustainable Energy*, vol. 8, no. 1, pp. 13-22, 2017.
- [11] Y. Z. Gerdroodbari, R. Razzaghi, and F. Shahnia, "Decentralized control strategy to improve fairness in active power curtailment of PV inverters in low-voltage distribution networks," *IEEE Transactions on Sustainable Energy*, vol. 12, no. 4, pp. 2282-2292, 2021.
- [12] E. Demirok, P. C. González, K. H. B. Frederiksen, D. Sera, P. Rodriguez, and R. Teodorescu, "Local reactive power control methods for overvoltage prevention of distributed solar inverters in low-voltage grids," *IEEE Journal of Photovoltaics*, vol. 1, no. 2, pp. 174-182, 2011.
- [13] S.-B. Kim and S.-H. Song, "A hybrid reactive power control method of distributed generation to mitigate voltage rise in low-voltage grid," *Energies*, vol. 13, no. 8, 2020.
- [14] A. Samadi, R. Eriksson, L. Söder, B. G. Rawn, and J. C. Boemer, "Coordinated active power-dependent voltage regulation in distribution grids with PV systems," *IEEE Transactions on Power Delivery*, vol. 29, no. 3, pp. 1454-1464, 2014.
- [15] A. Samadi, E. Shayesteh, R. Eriksson, B. Rawn, and L. Söder, "Multi-objective coordinated droop-based voltage regulation in distribution grids with PV systems," *Renewable Energy*, vol. 71, pp. 315-323, 2014.
- [16] C. Zhang, Y. Xu, Y. Wang, Z. Y. Dong, and R. Zhang, "Three-stage hierarchically-coordinated voltage/var control based on PV inverters considering distribution network voltage stability," *IEEE Transactions on Sustainable Energy*, vol. 13, no. 2, pp. 868-881, 2022.
- [17] Y. Xu, Z. Y. Dong, R. Zhang, and D. J. Hill, "Multi-timescale coordinated voltage/var control of high renewable-penetrated distribution systems," *IEEE Transactions on Power Systems*, vol. 32, no. 6, pp. 4398-4408, 2017.
- [18] S. Xu, Y. Xue, and L. Chang, "Review of power system support functions for inverter-based distributed energy resources-standards, control algorithms, and trends," *IEEE Open Journal of Power Electronics*, vol. 2, pp. 88-105, 2021.
- [19] C. Zhang and Y. Xu, "Hierarchically-coordinated voltage/VAR control of distribution networks using PV inverters," *IEEE Transactions on Smart Grid*, vol. 11, no. 4, pp. 2942-2953, 2020.
- [20] O. Ceylan, S. Paudyal, and I. Pisica, "Nodal sensitivity-based smart inverter control for voltage regulation in distribution feeder," *IEEE Journal of Photovoltaics*, vol. 11, no. 4, pp. 1105-1113, 2021.
- [21] A. Momeneh, M. Castilla, J. Miret, P. Martí, and M. Velasco, "Comparative study of reactive power control methods for photovoltaic inverters in low-voltage grids," *IET Renewable Power Generation*, vol. 10, no. 3, pp. 310-318, 2016.
- [22] "American National Standard for Electric Power Systems and Equipment Voltage Ratings (60 Hz)," *American National Standards Institute (ANSI)*, 2016.
- [23] L. L. Lai, J. T. Ma, R. Yokoyama, and M. Zhao, "Improved genetic algorithms for optimal power flow under both normal and contingent operation states," *International Journal of Electrical Power & Energy Systems*, vol. 19, no. 5, pp. 287-292, 1997/06 1997.
- [24] C. Kuster, Y. Rezgui, and M. Mourshed, "Electrical load forecasting models: A critical systematic review," *Sustainable Cities and Society*, vol. 35, pp. 257-270, 2017.
- [25] A. R. Jordehi, "How to deal with uncertainties in electric power systems? A review," *Renewable and Sustainable Energy Reviews*, vol. 96, pp. 145-155, 2018.
- [26] Y. M. Atwa, E. F. El-Saadany, M. M. A. Salama, and R. Seethapathy, "Optimal renewable resources mix for distribution system energy loss minimization," *IEEE Transactions on Power Systems*, vol. 25, no. 1, pp. 360-370, 2010.
- [27] P. Kayal and C. K. Chanda, "Optimal mix of solar and wind distributed generations considering performance improvement of electrical distribution network," *Renewable Energy*, vol. 75, pp. 173-186, 2015.
- [28] M. R. Elkadeem, M. Abd Elaziz, Z. Ullah, S. Wang, and S. W. Sharshir, "Optimal planning of renewable energy-integrated distribution system considering uncertainties," *IEEE Access*, vol. 7, pp. 164887-164907, 2019.
- [29] Z. Ullah, S. Wang, J. Radosavljevic, and J. Lai, "A solution to the optimal power flow problem considering WT and PV generation," *IEEE Access*, vol. 7, pp. 46763-46772, 2019.
- [30] M. K. C. Marwali, M. Haili, S. M. Shahidehpour, and K. H. Abdul-Rahman, "Short term generation scheduling in photovoltaic-utility grid with battery storage," *IEEE Transactions on Power Systems*, vol. 13, no. 3, pp. 1057-1062, 1998.
- [31] R.-H. Liang and J.-H. Liao, "A fuzzy-optimization approach for generation scheduling with wind and solar energy systems," *IEEE Transactions on Power Systems*, vol. 22, no. 4, pp. 1665-1674, 2007.
- [32] W. H. Kersting, *Distribution System Modeling and Analysis*, 4 ed. Boca Raton : Taylor & Francis, CRC Press, 2017.
- [33] H. Ahmadi, J. R. Martí, and A. v. Meier, "A linear power flow formulation for three-phase distribution systems," *IEEE Transactions on Power Systems*, vol. 31, no. 6, pp. 5012-5021, 2016.
- [34] J. Radosavljevic, *Metaheuristic Optimization in Power Engineering*. London, UK: Institution of Engineering and Technology, 2018.
- [35] EPRI. *Open Distribution System Simulator, Sourceforge.Net.*: <http://sourceforge.net/projects/electricdss/files/>.
- [36] L. Wen, L. Gao, X. Li, and L. Zhang, "Free Pattern Search for global optimization," *Applied Soft Computing*, vol. 13, no. 9, pp. 3853-3863, 2013.
- [37] R. Hooke and T. A. Jeeves, "'Direct Search' solution of numerical and statistical problems," *Journal of the ACM (JACM)*, vol. 8, no. 2, pp. 212-229, 1961.
- [38] S. Conti, A.M. Gerco, and S. Raiti, "Voltage sensitivity analysis in MV distribution networks," presented at the The 6th WSEAS/IASME Int. Conf. on Electric Power Systems, High Voltages, Electric Machines, Tenerife, Spain, December 16-18, 2006.
- [39] Test Feeder Working Group of the Distribution System Analysis Subcommittee. (1/5/2022). *IEEE PES Test Feeder* [Online]. Available: <https://cmt.ee.utoronto.ca/pes-testfeeders/resources/>.
- [40] K. P. Schneider *et al.*, "Analytic considerations and design basis for the IEEE distribution test feeders," *IEEE Transactions on Power Systems*, vol. 33, no. 3, pp. 3181-3188, 2018.
- [41] S. S. Alkaabi, H. H. Zeineldin, and V. Khadkikar, "Short-term reactive power planning to minimize cost of energy losses considering PV systems," *IEEE Transactions on Smart Grid*, vol. 10, no. 3, pp. 2923-2935, 2019.
- [42] *Power Quality Application Guide, Voltage disturbances EN 50160*, 2004.
- [43] I. Richardson and M. Thomson. Integrated domestic electricity demand and PV micro-generation model, Loughborough University [Online] Available: <https://hdl.handle.net/2134/7773>



**F. M. Aboshady** (Senior Member, IEEE) received the B.Sc. and M.Sc. degrees in electrical engineering from Tanta University, Egypt, in 2010 and 2014, respectively, and the Ph.D. degree in electrical and electronic engineering from the University of Nottingham, U.K., in 2019. He is a Research Fellow with Brunel University London and an Assistant Professor with Tanta University. His research interests include fault location

strategies, protection of electric grids, electric vehicles, and integration of renewable energy systems.

His current research interests include transmission system operation, smart grids, and power system modeling and analysis



**Oguzhan Ceylan** received the M.Sc. and Ph.D. degrees in computational science and engineering from Istanbul Technical University, Istanbul, Turkey, in 2003 and 2012, respectively. From 2013 to 2015, he was a Postdoctoral Researcher with the University of Tennessee, Knoxville, TN, USA. He is currently an associate professor at Marmara University, Electrical and Electronics Engineering Department. His research interests include smart grids, integration of renewable into distribution systems, and intelligent optimization methods.



**Aydogan Ozdemir** was born in Artvin, Turkey in January 1957. He received B.Sc., M.Sc., and Ph.D. degrees in electrical engineering from Istanbul Technical University, Istanbul, Turkey, in 1980, 1982, and 1990, respectively. He is currently a full-time professor at the same university and the manager of Fuat Kulunk High Voltage Laboratory. His current research interests are in the area of high voltage engineering and electric

power systems with an emphasis on reliability assessment, distributed generation, and intelligent system applications.



**Ioana Pisica** is an Associate Professor in Power Systems and member of the Brunel Interdisciplinary Power Systems Research Centre at Brunel University London. Ioana has been involved in agent-based modelling, smart metering communications and analysis of large amounts of data from smart meters with the aim to achieve energy efficiency. Her research interests include power systems management and operation optimization, renewable energy

systems, power quality, and energy efficiency in the built environment and industry.



**Ahmed F. Zobaa** (Senior Member, IEEE) received B.Sc. (Hons.), M.Sc., and Ph.D. degrees in electrical power and machines from Cairo University, Cairo, Egypt, in 1992, 1997, and 2002, respectively. Between 2007 and 2010, he was a Senior Lecturer in renewable energy with the University of Exeter, Exeter, U.K. He was also an Instructor with Cairo University between 1992 and 1997, a Teaching Assistant between 1997 and 2002, an Assistant

Professor between 2003 to 2008, and an Associate Professor from 2008 and 2013, where he has also been a Professor (on leave) since December 2013. He is currently a Reader in power systems and a Full Member of the Institute of Energy Futures, Brunel University London, London, U.K. His main areas of expertise are power quality, (marine) renewable energy, smart grids, energy efficiency, and lighting applications, Dr Zobaa is currently a Senior Fellow of the Higher Education Academy of U.K., and a Fellow of the IET, the Energy Institute of the U.K., the Chartered Institution of Building Services Engineers, the Institution of Mechanical Engineers, the Royal Society of Arts, the African Academy of Science, and the Chartered Institute of Educational Assessors. He is a member of the International Solar Energy Society, the European Power Electronics and Drives Association, and the IEEE Standards Association. He is the Editor-in-Chief for the International Journal of Renewable Energy Technology, International Journal of Electrical Engineering & Education, and Technology and Economics of Smart Grids and Sustainable Energy. He is also an Editorial Board member, Editor, Associate Editor, and Editorial Advisory Board member for many international journals. He is a registered Chartered Engineer, Chartered Energy Engineer, European Engineer, and International Professional Engineer, and is a registered member of the Engineering Council U.K., Egypt Syndicate of Engineers, and the Egyptian Society of Engineers.



**Gareth A. Taylor** received the B.Sc. degree from the University of London, London, U.K., in 1987, and the M.Sc. and Ph.D. degrees from the University of Greenwich, London, in 1992 and 1997, respectively. He was the National Grid U.K. Post-Doctoral Scholar with Brunel University London, Uxbridge, U.K., from 2000 to 2003, where he is currently a Professor and Head of the Electronic and Electrical Engineering Department. He is Director of the Brunel Interdisciplinary Power Systems Research Centre.